UPPSALA UNIVERSITET

Digital Comprehensive Summaries of Uppsala Dissertations from the Faculty of Medicine 1429

Towards Clinical Implementation of Dynamic Positron Emission Tomography in Neurodegenerative Diseases

MY JONASSON

ACTA UNIVERSITATIS UPSALIENSIS UPPSALA 2018

ISSN 1651-6206
ISBN 978-91-513-0238-6
urn:nbn:se:uu:diva-341786

Dissertation presented at Uppsala University to be publicly examined in Skoogsalen, Akademiska Sjukhuset, Ing 79, Uppsala, Friday, 6 April 2018 at 09:15 for the degree of Doctor of Philosophy. The examination will be conducted in English. Faculty examiner: Associate professor Michel Koole (Department of Imaging & Pathology, University of Leuven, Belgium).

Abstract

Jonasson, M. 2018. Towards Clinical Implementation of Dynamic Positron Emission Tomography in Neurodegenerative Diseases. *Digital Comprehensive Summaries of Uppsala Dissertations from the Faculty of Medicine* 1429. 55 pp. Uppsala: Acta Universitatis Upsaliensis. ISBN 978-91-513-0238-6.

Alzheimer's disease (AD) and Parkinson's disease (PD) are the two most common neurodegenerative disorders worldwide. Positron emission tomography (PET), together with suitable biomarkers, can aid in the clin-ical evaluation as well as in research investigations of these diseases. Straightforward and quantitative assessments of the parameters of inter-est estimated on a voxel-level, as parametric images, are possible when PET data is acquired over time. Prerequisites to facilitate clinical use of dynamic PET are simplified analysis methods and scan protocols suita-ble for clinical routine.

The aim of this thesis was to validate simplified analysis methods, suitable for clinical use, for quantification of dopamine transporter (DAT) availability in patients with parkinsonism using [^{11}C]PE2I PET and tau accumulation in AD patients with [^{18}F]THK5317 PET.

The included subjects comprised of both healthy controls and pa-tients with parkinsonism, AD or mild cognitive impairment and each subject underwent a dynamic PET scan with either [^{11}C]PE2I or [^{18}F]THK5317. Models for quantitative voxel-based analysis, resulting in parametric images of tracer binding and overall brain function, were validated in both patients and controls. These parametric methods were compared to region-based values acquired using both plasma- and refer-ence-input models. Clinically feasible scan durations were evaluated for both [^{11}C]PE2I and [^{18}F]THK5317, and a clustering method to obtain a reference time activity curve directly from the dynamic PET data was validated. Furthermore, images of DAT availability and overall brain functional activity, generated from one single dynamic [^{11}C]PE2I PET scan, were compared to a dual-scan approach using [^{123}I]FP-CIT single photon emission computed tomography (SPECT) and [^{18}F]FDG PET, for differential diagnosis of patient with parkinsonism.

Study I-III supply valuable information on the feasibility of dynamic [^{11}C]PE2I in a clinical setting for differential diagnosis of parkinsonian disorders, by having easily accessible images of DAT availability and overall brain functional activity. The work in study IV-V showed that reference methods can be used for quantification of tau accumulation, and suggests that simplified analysis methods and shorter scan durations can be applied to further facilitate applications of dynamic [^{18}F]THK5317 PET.

Keywords: Positron emission tomography, PET, Molecular imaging, Quantification, Kinetic modelling, Parametric images, Alzheimer's disease, Parkinson's disease

My Jonasson, Department of Surgical Sciences, Radiology, Akademiska sjukhuset, Uppsala University, SE-75185 Uppsala, Sweden.

ISSN 1651-6206
ISBN 978-91-513-0238-6
urn:nbn:se:uu:diva-341786 (http://urn.kb.se/resolve?urn=urn:nbn:se:uu:diva-341786)

To Patric and Milo

List of Papers

This thesis is based on the following papers, which are referred to in the text by their Roman numerals.

I Jonasson, M., Appel, L., Engman, J., Frick, A., Nyholm, D., Askmark, H., Danfors, T., Sörensen, J., Furmark, T. and Lubberink, M. (2013) Validation of parametric methods for [^{11}C]PE2I positron emission tomography, *NeuroImage,* 74:172-178

II Appel, L., Jonasson, M., Danfors, T., Nyholm, D., Askmark, H., Lubberink, M. and Sörensen, J. (2015) Use of ^{11}C-PE2I PET in differential diagnosis of parkinsonian disorders, *Journal of Nuclear Medicine,* 56(2):234-242

III Jonasson, M., Appel, L., Danfors, T., Nyholm, D., Askmark, H., Frick, A., Engman, J., Furmark, T., Sörensen J. and Lubberink, M., (2017) Development of a clinically feasible [^{11}C]PE2I PET scan protocol for differential diagnosis of parkinsonism using supervised cluster analysis, *American Journal of Nuclear Medicine and Molecular Imaging*, 7(6):263-274

IV Jonasson, M., Wall, A., Chiotis, K., Saint-Aubert, L., Wilking, H., Sprycha, M., Borg, B., Thibblin, A., Eriksson, J., Sörensen, J., Antoni, G., Nordberg A. and Lubberink, M. (2016) Tracer kinetic analysis of *(S)*-^{18}F-THK5117 as a PET tracer for assessing tau pathology, *Journal of Nuclear Medicine,* 57(4):574-581

V Jonasson, M., Wall, A., Chiotis, L., Leuzy, A., Eriksson, J., Antoni, G., Nordberg, A. and Lubberink, M. Optimal timing of tau pathology imaging and automatic extraction of a reference region using dynamic [^{18}F]THK5317, *Manuscript*

List of Non-Thesis Publications

I Frick, A., Åhs, F., Linnman, C., Jonasson, M., Appel, L., Lubberink, M., Långström, B., Fredrikson, M. and Furmark, T. (2015) Increased neurokinin-1 receptors availability in the amygdala in social anxiety disorder: a positron emission tomography study with [^{11}C]GR205171, *Translational Psychiatry*, 5:e597

II Frick, A., Åhs, F., Engman, J., Jonasson, M., Alaie, I., Björkstrand, J., Frans, Ö., Faria, V., Linnman, C., Appel, L., Wahlstedt, K., Lubberink, M., Fredrikson, M. and Furmark, T. (2015) Serotonin synthesis and reuptake in social anxiety disorder: A positron emission tomography Study, *JAMA Psychiatry,* 72(8):794-802

III Lubberink, M., Golla, SSV., Jonasson, M., Rubin., Glimelius, B., Sörensen, J. and Nygren, P., (2015) ^{15}O-Water PET study of the effect of Imatinib, a selective platelet-derived growth factor receptor inhibitor, versus anakinra, an IL-1R antagonist, on water-perfusable tissue fraction in colorectal cancer metastases. *Journal of Nuclear Medicine*, 56(8):1144-1149

IV Chiotis, K., Saint-Aubert, L., Savitcheva, I., Jelic, V., Andersen, P., Jonasson, M., Eriksson, J., Lubberink, M., Almkvist, O., Wall, A., Antoni, G. and Nordberg, A. (2016) Imaging in-vivo tau pathology in Alzheimer's disease with THK5317 in a multimodal paradigm, *European Journal of Nuclear Medicine and Molecular Imaging,* 43(9):1686-1699

V Frick, A., Åhs, F., Palmquist, ÅM, Pissiota, A., Wallenquist, U., Fernandez, M., Jonasson, M., Appel, L., Frans, Ö., Lubberink, M., Furmark, M., Furmark, T., von Knorring, L. and Fredrikson, M. (2016) Overlapping expression of serotonin transporters and neurokinin-1 receptor in posttraumatic stress disorder: a multi-tracer PET study. *Molecular Psychiatry* 21(10):1400-1407

VI Frick, A., Åhs, F., Appel, L., Jonasson, M., Wahlstedt, K., Bani, M., Merlo Pich, E., Bettica, P., Långström, B., Lubberink, M., Fredrikson and M., Furmark, T. (2016) Reduced serotonin synthesis and regional cerebral blood flow after anxiolytic treatment of social anxiety disorder. *European Neuropsychopharmacology,* 26(11):1775-1783

VII Chiotis K., Saint-Aubert, L., Rodriguez-Vieitez, E., Leuzy, A., Almkvist, O., Savitcheva, I., Jonasson, M., Lubberink, M., Wall, A., Antoni, G. and Nordberg, A. (2017) Longitudinal changes of tau PET in relation to hypometabolism in prodromal and Alzheimer's disease dementia, *Molecular Psychiatry*, In press

VIII Heurling, K., Leuzy, A., Jonasson, M., Frick, A., Zimmer, E.R., Nordberg, A. and Lubberink, M. (2017) Quantitative positron emission tomography in brain research, *Brain Research,* 1670:220-234

IX Leuzy, A., Rodriguez-Vieitez, E., Saint-Aubert, L., Chiotis, K., Almkvist, O., Savitcheva, I., Jonasson, M., Lubberink, M., Wall, A. and Nordberg, A. (2017) Longitudinal uncoupling of cerebral perfusion, glucose metabolism, and tau deposition in Alzheimer's disease, *Alzheimer's & Dementia,* In press

Cover image
Artwork by Helena Mutanen, *Lock Pick,* 2009

Contents

Abbreviations

1TCM	One tissue compartment model
2TCM	Two tissue compartment model
AD	Alzheimer's disease
BP_{ND}	Binding potential
Bq	Becquerel
COV	Coefficient of variation
CSF	Cerebrospinal fluid
DVR	Distribution volume ratio
HC	Healthy control
MCI	Mild cognitive impairment
MRI	Magnetic resonance imaging
MRTM	Multilinear reference tissue model
MSA	Multiple system atrophy
p.i.	Post-injection
PD	Parkinson's disease
PET	Positron emission tomography
R_1	Relative tracer delivery
SAD	Social anxiety disorder
RPM	Receptor parametric mapping
SPECT	Single photon emission computed tomography
SRTM	Simplified reference tissue model
SUVR	Standard uptake value ratio
SVCA	Supervised cluster analysis
TAC	Time activity curve
TE	Transient equilibrium
VOI	Volume of interest
V_T	Volume of distribution

Introduction

Alzheimer's disease (AD) and Parkinson's disease (PD) are the two most common neurodegenerative disorders worldwide. Functional molecular imaging methods such as positron emission tomography (PET), using different radiotracers, can aid in the clinical evaluation as well as in research investigations of these diseases. Parkinsonism is a group of neurodegenerative disorders, where PD is the most common one, but with several other disorders that are often misdiagnosed. The use of PET with [^{11}C]PE2I, a tracer that binds to dopamine transporters (DAT), can support the differentiation between parkinsonian disorders since the central dopaminergic and overall brain functional activity are altered differently. AD is characterized by a cascade of complex pathophysiologic processes, for example accumulation of tau proteins, which is closely associated with neurodegeneration and cognitive impairment. [^{18}F]THK5317 is a tau-specific PET tracer, showing high retention in patients with AD and can possibly aid in the diagnosis.

To facilitate clinical use of dynamic PET there are some prerequisites: straightforward visual assessments, as parametric images, where the parameters of interest are estimated for each voxel, simplified analysis methods and scan protocols suitable for clinical routine. This thesis aims to evaluate simplified methods for acquisition and quantification of dynamic PET data for clinical use in neurodegenerative diseases, with focus on AD and PD.

Background

Positron emission tomography

Basic principles

PET is a molecular imaging technique used for investigations of a variety of physiological and molecular functions *in-vivo* by measuring the distribution of radiolabelled compound, so called radioligands or tracers, after intravenous injection. The PET tracers are labelled with short-lived radioisotopes that decay by positron emission and the most commonly used positron emitting nuclides are fluorine-18 (^{18}F), carbon-11 (^{11}C) and oxygen-15 (^{15}O). When the radioisotope decays, the emitted positron travels a very short distance from the initial decay site before it interacts with an electron and a positron-electron annihilation occurs. This produces two photons with an energy of 511 keV, that are emitted simultaneously in opposite direction and detected by an opposing pair of detectors in the PET scanner. A simplified drawing of this process is showed in Figure 1.

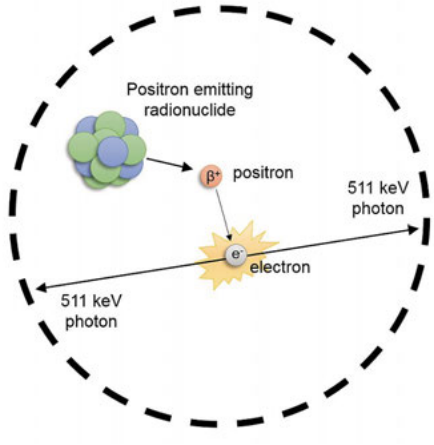

Figure 1. Schematic drawing of the positron emission and annihilation, resulting in two 511 keV photons. The ring represents the PET scanner where the photons are detected by two opposing detectors.

The PET system consists of rings of detector blocks where each detector element is operating in coincidence with multiple elements on the opposite side to record the annihilation photons. The detector blocks commonly consist of

bismuth germinate (BGO) or lutetium oxyorthosilicate (LSO) scintillation crystals, segmented into arrays of smaller elements, and photomultiplier tubes. The axial field of view is determined by the extent of the detectors and is typically in the range of 15-25 cm. The near simultaneous detection of the annihilation photons by the PET system makes it possible to determine a line between the detection sites, which gives an indication of where in the body the positron emission occurred and defines the volume from where they were emitted. The coincidence events collected by the PET detectors are reconstructed into a tomographic image. The reconstructed PET images are corrected for attenuation, random coincidences, scattered radiation, dead time and physical decay of the radioisotope, and show the distribution of the tracer as the radioactivity concentration (Bq/mL). The resolution of the PET image is in the order of mm, and is affected by several different parameters such as the size of the detector elements, the range that the positron travels before the annihilation occurs, which is dependent on the positron energy, and the non-collinearity of the emitted photons, meaning that due to residual momentum of the positron and the electron, the photons are not exactly emitted at 180-degree opposing direction [1].

Quantification

In order to quantify the physiological parameters of interest, such as the binding of the tracer to a specific target or the blood flow, from the PET image, there is a need for information regarding the rate of change of the radioactivity concentration over time. Collecting the data in separate time frames, as a dynamic scan, will show how the concentration of the tracer in tissue changes throughout the course of the PET study, as illustrated in Figure 2A. From the dynamic scan, time activity curves (TACs) can be obtained, showing the radioactivity concentration over time in a specific volume of interest (VOI) or a voxel. The shape of the TAC is dependent on the properties of the tracer and the tissue as seen in Figure 2B.

The measured radioactivity concentration in the PET image is a combination of the different states of the tracer in the tissue, such as radioactivity in the blood within the tissue, tracer bound to its intended target or tracer bound to other entities. These states are commonly depicted as different compartments and there are different approaches to differentiate between the compartments and estimate the parameters of interest.

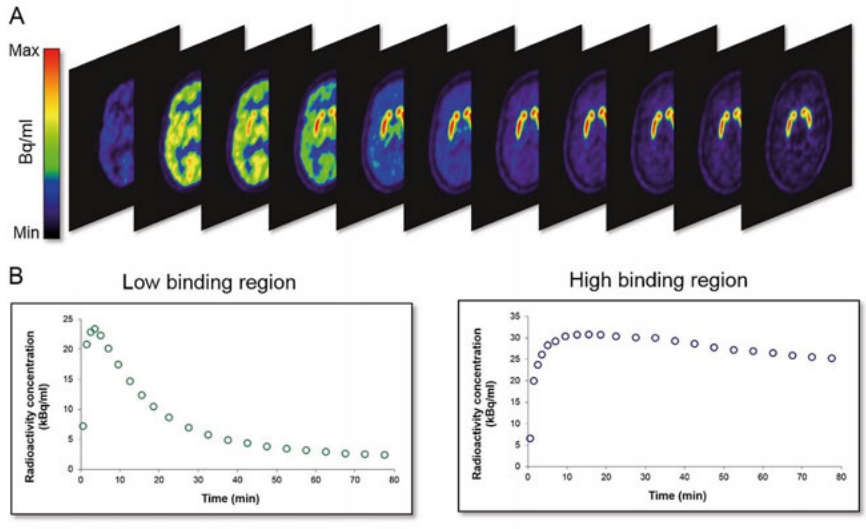

Figure 2. A) Examples of a range of frames from a dynamic [^{11}C]PE2I brain PET scan with a duration of 80 min. Each frame is showing the distribution of tracer in the brain, while the collection of frames shows the temporal changes of tracer concentration. B) Time activity curves, showing radioactivity concentration over time in a region with high and with no specific binding.

Compartmental modelling

To calculate the parameters of interest, there is a need for a mathematical model that describes the measured radioactivity concentration over time. The most commonly used compartment models are the two tissue compartment models (2TCM) and the one tissue compartment model (1TCM), shown in Figure 3A and B respectively.

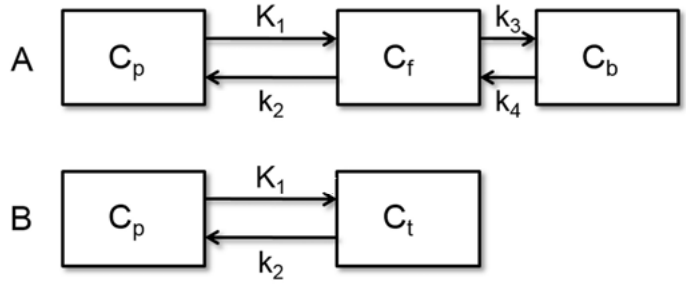

Figure 3. Schematic drawing of A) the two tissue compartment model and B) the one tissue compartment model. C_p, C_f, C_b and C_t represents the radioactive concentration in the different compartments and K_1, k_2, k_3 and k_4 represents the rate constants.

C_p, is the radioactivity concentration in arterial plasma, which is measured by taking arterial blood samples during the PET scan. C_f is the free and non-specifically bound tracer in the tissue, while C_b represents the tracer bound to the target. The different rate constants K_1, k_2, k_3 and k_4 represent the exchange of tracer between plasma and tissue, and between the different compartments. The signal measured by PET in a certain VOI or voxel is a combination of C_f and C_b plus a fractional blood volume in tissue. In case of regions with no specific binding, or when the free and bound tracer are assumed to be indistinguishable due to fast exchange between the compartments, the model can be simplified to a 1TCM. The compartment models can be described by differential equations and the parameters of interest can be derived using non-linear regression analysis. The parameters of interest are often the non-displaceable binding potential (BP_{ND}), where $BP_{ND}=k_3/k_4$ [2]. BP_{ND} is not always possible to be determined accurately, instead, the distribution volume (V_T) can be estimated which under equilibrium equals $V_T=K_1/k_2$ for the 1TCM and $V_T=(K_1/k_2)(1+k_3/k_4)$ for the 2TCM. An alternative approach for parameter estimation is the Logan plot [3], a graphical analysis represented by linear equations that can be solved graphically where the resulting slope = V_T.

Reference region

A reference region is a region that is devoid of target, that is, with no specific binding of the tracer, and with a non-specific distribution volume similar to the target region. If it is not possible to determine BP_{ND} directly by k_3/k_4, it can be estimated as the ratio of the distribution volumes in the target tissue and the reference tissue minus one. However, this still requires arterial blood sampling. Arterial blood sampling during the PET investigation is invasive, labour intensive and sometimes not feasible. It is possible to eliminate the dependency of the model on the plasma input function if there is a proper reference region in the brain. A TAC from the reference VOI can then be used as an indirect input function to a reference tissue model. The simplified reference tissue model (SRTM) [4], as illustrated in Figure 4, is the most commonly used reference tissue model. In addition to the two requirements mentioned before, SRTM requires that both reference and target TACs can be approximated by the 1TCM. SRTM estimates three parameters, BP_{ND}, k_2 and R_1, where R_1 is the relative tracer delivery, which is closely related to blood flow, assuming that tracer extraction is uniform throughout the brain. A further simplification of SRTM can be made by fixing k_{2a} to a pre-defined value, and by so, reducing the number of estimated parameters to two (SRTM2) [5], and both models can be linearized using a set of basis functions, receptor parametric mapping (RPM and RPM2) [6]. The Logan graphical approach can also be calculated using a reference region instead of a plasma input function and the slope of the graphical analysis then corresponds to the ratio of volumes of distribution in the target and the reference region (DVR) [7]. Another reference tissue approach is the multilinear reference tissue models (MRTM),

solved using multilinear regression after a certain equilibrium time. There are three versions of MRTM, and as for RPM, either three or two parameters can be estimated (MRTM, MRTMo, MRTM2 [8, 9].

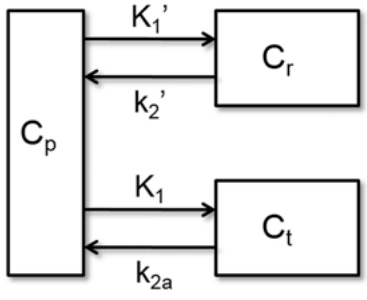

Figure 4. The simplified reference tissue model (SRTM) where C_p, C_r and C_t represent the radioactivity concentration in the different compartments and K_1, K_1', k_{2a} and k_2' represent the different rate constants.

VOI-based reference

Most commonly, the reference region VOI, as well as other regions of interest, is obtained by manual definition of the volume. Due to the poor anatomical information in the PET images, this is usually performed on co-registered images from other imaging modalities such as computed tomography (CT) or magnetic resonance imaging (MRI), after which the VOIs are transferred to the PET images. This process is both time consuming and prone to inter-user variability. Automated software based on pre-defined VOI template, matched to the individual subjects MRI scan by non-rigid co-registration, can overcome these limitations and the advantage is that a whole set of VOIs can be defined simultaneously.

SVCA-based reference

An automatic way to define the reference region VOI directly from the dynamic PET data, without the need for a structural MRI for manual or template-based region definition, is the supervised cluster analysis (SVCA) method. The SVCA algorithm segments voxels in the dynamic PET volume based on the shape of their TACs with no spatial constraint, i.e. the whole brain is considered. Voxels with kinetic behaviour most resembling the TACs of the proposed reference region are included in the reference VOI. The SVCA method has demonstrated to be a robust and reliable alternative as an automatic way of extracting a reference region in previous studies for *(R)*-[^{11}C]PK1119 [10, 11], [^{11}C]PIB [12], [^{11}C](R)-rolipram [13] and [^{11}C]TMSX [14].

Parametric images

In addition to estimating the parameters of interest on a VOI-basis, the estimation can also be performed on a voxel-level. This results in a spatial map,

also known as a parametric image, of the parameters of interest and gives a straightforward visualisation of the parameter estimates. Using a standard non-linear regression analysis for the parameter estimations is very time consuming and sensitive to noise, and thus not practical for voxel-based analysis. Instead, linearization of the models such as the RPM- and MRTM-methods for calculation of BP_{ND} and R_1 parametric images, as well as voxel-level estimation of DVR using reference Logan, are implemented. Quantification of dynamic PET data, where both the specific binding and flow characteristics of the tracer are assessed, resulting in BP_{ND} and R_1 [15, 16], can make dynamic PET investigations even more attractive for clinical use.

Semiquantitative measures

A semi-quantitative estimate of the binding is the standard uptake value ratio (SUVR), relating the radioactivity concentration in the target region to that in the reference region. The optimal time for assessment of SUVR, in terms of agreement with BP_{ND}, is at transient equilibrium (TE) which is the time when the specific binding curve, calculated as the different between target and reference tissue, peaks [17] and theoretically BP_{ND} equals SUVR-1. Since SUVR can be obtained using a static scan, and can be estimated on a VOI-basis as well as on a voxel-level, it is an attractive alternative to the more advanced methods requiring dynamic scanning.

PET in Parkinson's disease and Alzheimer's disease

The application of PET in brain research is growing and PET is used in a wide variety of applications within neurology [18]. This includes investigation of pathophysiological processes, disease diagnosis and progression, monitoring treatment response, drug development as well as increasing the understanding of normal brain functions. In this thesis, the focus lies on PET in neurodegenerative diseases, specifically parkinsonian disorders and Alzheimer's disease, and the clinical applicability of dynamic PET, utilizing its full potential in these disorders.

Parkinsonian disorders

Parkinsonism is a clinical syndrome characterized by the typical motor symptoms such as bradykinesia, rigidity, tremor and postural instability. There are also several non-motor symptoms associated with parkinsonism, for example depression, cognitive impairment and sleep disorders [19]. The different parkinsonian disorders include Parkinson's disease, which is the most common one, and other neurological conditions, such as multiple system atrophy (MSA), progressive supranuclear palsy, dementia with Lewy bodies and corticobasal degeneration, with overlapping clinical symptoms. There are also

some non-neurodegenerative causes for PD-like symptoms, such as vascular parkinsonism and drug-induced parkinsonism. Although progression and pathology differs between different parkinsonian syndromes, an unambiguous diagnosis can be difficult to achieve based on the clinical symptoms, especially at early stages of the disease [20, 21].

Several brain regions and neurotransmitter systems are affected in parkinsonism where the degeneration of dopaminergic neurons in the nigrostriatal pathway, which is responsible for the classic motor symptoms in PD, are the most prominent. PET can aid in the differentiation between parkinsonian disorders because the central dopaminergic and overall brain functional activity are altered differently [22-27]. There are several PET tracers targeting the dopaminergic system such as [^{11}C]raclopride [28], [^{18}F]FDOPA [29], [^{18}F]FP-CIT [30] and [^{18}F]FE-PE2I [31], as well as the single photon emission computed tomography (SPECT) tracer [^{123}I]FP-CIT [32] and [^{123}I]PE2I [33]. To aid in the differentiation between various parkinsonian disorders, [^{18}F]FDG PET is commonly used to examine the metabolic activity in the brain which is closely related to the overall brain function. However, the focus of this thesis, when targeting patients with parkinsonism will be the dopamine transporter (DAT) PET tracer [^{11}C]PE2I. DAT is a transmembrane protein responsible for the reuptake of dopamine in the synaptic cleft. Decreased DAT availability is associated with different neurodegenerative disorders such as Parkinson's disease [34, 35].

[^{11}C]PE2I

The cocaine analog N-(3-iodoprop-2E-enyl)-2β-carbomethoxy-3β-(4-methylphnyl)nortropane (PE2I) has shown an excellent binding to DAT, in both *in-vitro* autoradiography studies, using [^{125}I]PE2I [36] and *in-vivo* PET studies with [^{11}C]PE2I [37-39]. It has shown a high accumulation in striatum, where the concentration of DAT is high, an intermediate binding in midbrain, and no or very little specific binding in the cerebellum. The high selectivity of [^{11}C]PE2I for DAT offers a high potential for *in-vivo* exploration of DAT function [40] and has been used in both research studies [41, 42] and in clinical trials [43, 44]. [^{11}C]PE2I PET studies can thus be a valuable tool for early detection and differentiation of neurological disorders where changes in DAT concentration are involved, such as parkinsonism. In Figure 5, examples of [^{11}C]PE2I PET images 60-80 min post-injection (p.i.) are shown from one patient with PD and one healthy control (HC).

It has been shown that reference tissue methods on a VOI-basis using SRTM, although underestimating BP_{ND}, show a high correlation to plasma-input compartment models [37, 45] and also a good reproducibility and reliability in test-retest studies [38]. [^{11}C]PE2I BP_{ND} has previous been estimated on a voxel-level [46-48], but no extensive validation of parametric methods

had been performed for [^{11}C]PE2I. Previous studies have proposed an acquisition time of 70 up to 120 min for [^{11}C]PE2I to be able to robustly determine DAT binding in the striatum [37-39, 45].

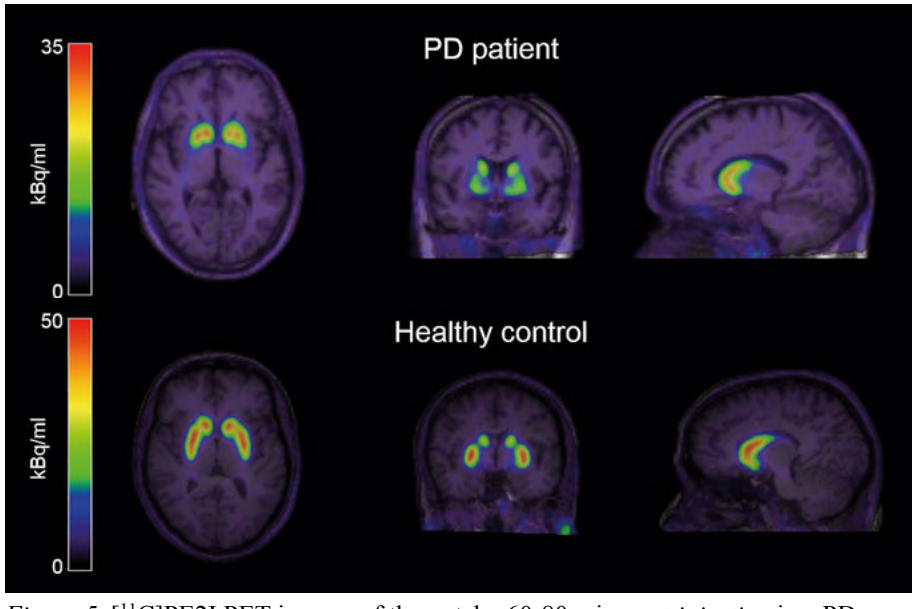

Figure 5. [^{11}C]PE2I PET images of the uptake 60-80 min *post-injection* in a PD patient, top row, and a healthy control, bottom row. The reduced DAT availability is clearly visible in the PD patient compared to the control. PET images are fused with the subjects' MRI images.

Alzheimer's disease

AD is an irreversible neurodegenerative disease that is characterized by progressive decline in cognition, personality changes and other symptoms common for dementia. As for PD, differential diagnosis between different causes of dementia can be difficult based on the clinical symptoms alone. The development of molecular imaging has provided valuable biomarkers for accurate and early detection of AD and has also led to proposal of new diagnostic criteria [49, 50]. There are several complex pathophysiological processes that characterizes AD, such as deposition of amyloid-beta plaques, tau filaments in the form of neurofibrillary tangles and neurodegeneration. Several tracers that bind to amyloid-beta plaques have been investigated and are widely used in both clinical settings and research studies, such as [^{11}C]PIB [51], [^{18}F]flutemetamol and [^{18}F]florbetapir. However, the amyloid pathology plateaus quite early in the progression of the disease [52] and PET-imaged amyloid pathology appeared not to correlate with clinical symptoms [53]. Because of the close association between tau pathology, neurodegeneration and cognitive impairment [54] there is an increasing interest in developing PET tracers

that binds specifically to tau [55, 56]. A number of them has undergone tracer kinetic studies in humans, such as [^{18}F]THK5351 [57], [^{11}C]PBB3 [58] and [^{18}F]AV1451 [59]. The part of this thesis targeting patients with AD will focus on quantification of the PET tracer [^{18}F]THK5317.

[^{18}F]THK5317

One of the promising tau tracers developed in recent years is 6-[(3-[^{18}F]fluoro-2-hydroxy)propoxy]-2-(4-methylaminophenyl)quinoline ([^{18}F]THK5117), which has shown good affinity for the tau protein aggregates and fast uptake and clearance [60]. [^{18}F]THK5117 is a racemic compound and for further analysis of the assessment of tau accumulation the *S*-enantiomeric form was used (*(S)*-[^{18}F]TKH5117) which from here on will be referred to as [^{18}F]THK5317. Examples of [^{18}F]THK5317 PET images 60-90 min p.i. in one AD patient and one HC are given in Figure 6.

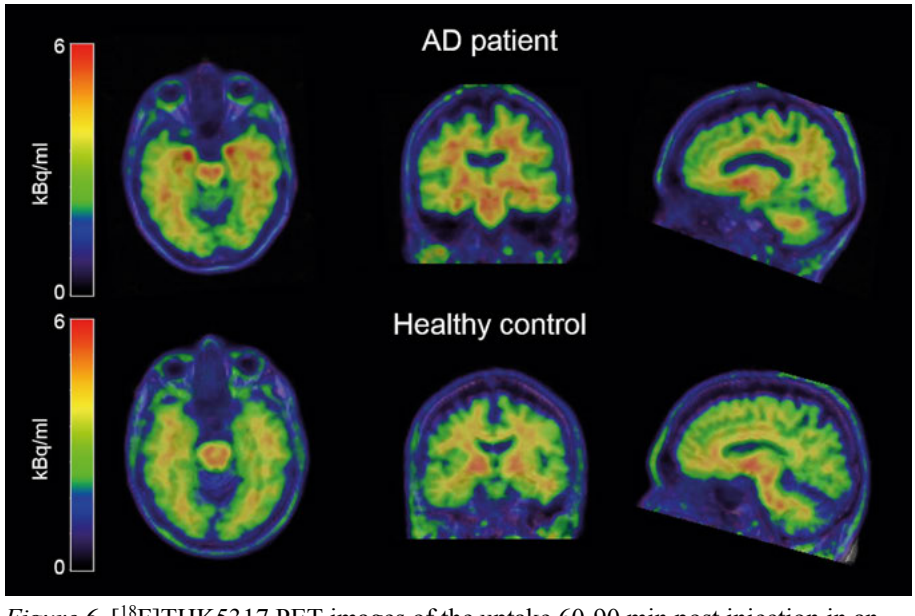

Figure 6. [^{18}F]THK5317 PET images of the uptake 60-90 min post injection in an AD patient, top row, and a healthy control, bottom row. PET images are fused with the subjects MRI images.

Aims of the thesis

The overall aims of this thesis were: 1) to facilitate clinical use of dynamic [^{11}C]PE2I PET by easy accessible images of DAT availability and overall functional activity for use in differential diagnosis of parkinsonian disorders, and 2) to evaluate models for quantification and simplified methods for assessment of tau accumulation in AD patients using dynamic [^{18}F]THK5317 PET.

More specifically, the aims of each study were the following:

I To validate different methods for producing parametric BP_{ND} and R_1 images of dynamic [^{11}C]PE2I data.

II To compare [^{11}C]PE2I R_1 and BP_{ND} images to imaging-based evaluation of parkinsonian disorders with [^{18}F]FDG PET and [^{123}I]FP-CIT SPECT.

III To investigate a shorter scan protocol for [^{11}C]PE2I and to validate a supervised cluster analysis method for automatic extraction of a reference time activity curve directly from the dynamic [^{11}C]PE2I data.

IV To evaluate different tracer kinetic models for quantitative analysis of [^{18}F]THK5317 binding to tau, based on plasma and reference tissue input data.

V To determine optimal timing for SUVR-1 and R_1 measures for [^{18}F]THK5317 and to validate a supervised cluster analysis method for automatic reference region extraction.

Materials and methods

Participants

This thesis is based on data from a total of 61 subjects, including healthy controls, subjects with social anxiety disorder (SAD) and patients with parkinsonism, AD or mild cognitive impairment (MCI). Briefly, the participants were included as follow: Paper I-III comprise of a set or subset of 16 patients with parkinsonism (10 women and 6 men, mean age 69 ± 6 years). In Paper I, 6 of these patients were included (5 women and 1 man, mean age 68 ± 6 years) together with 6 SAD subjects (3 women and 3 men, mean age 35 ± 11 years). Paper II included all 16 parkinsonism patients and paper III comprised of 12 of the patients with parkinsonism (7 women and 5 men, mean age 70 ± 6 years), 12 HC (4 women and 8 men, mean age 47 ± 8 years) and 5 additional healthy subjects (men, mean age 25 ± 4 years) included as a separate set of data for definition of kinetic classes in the SVCA algorithm. In paper IV, 5 AD patients (57-74 years) and 4 MCI patients (65-79 years) were included. Paper V comprise of a total of 9 AD patients (57-75 years) and 9 HC (21-71 years). Ten of the subjects (5 AD and 5 HC) were included for the analysis and remaining subjects were included for definition of SVCA kinetic classes. Patients were included based on their clinical diagnosis and each subject signed a written informed consent and the studies were approved by regional ethical review boards.

Data acquisition

All subjects underwent a dynamic PET scan, with either an 80 min [^{11}C]PE2I PET duration (Paper I-III) or a 60 or 90 min [^{18}F]THK5317 PET duration (Paper IV-V). All [^{11}C]PE2I and [^{18}F]THK5317 PET investigations were performed on an ECAT Exact HR+ scanner (Siemens/CTI, Knoxville) in 3D mode after a 10 min transmission scan with rotating ^{68}Ge rod sources for attenuation correction. The scans were reconstructed using ordered subset expectation maximization (OSEM) with 6 iterations and 8 subsets, and a 4 mm Hanning post-filter, with all appropriate corrections applied as included in the scanner software. Each subject received a T1-weighted structural MRI scan for VOI definition. In addition to the [^{11}C]PE2I scan, all patients in Paper II

also underwent a dual examination with a 10 or 20 min [^{18}F]FDG PET scan and a 30 min [^{123}I]FP-CIT SPECT scan.

[^{11}C]PE2I

Simultaneously with the start of the PET scan, 350-400 MBq of [^{11}C]PE2I was administered to the subjects in paper I-III. Data were acquired dynamically for 80 min and reconstructed into 22 frames of increasing duration (4 × 60, 2 × 120, 4 × 180 and 12 × 300 s). [^{11}C]PE2I was synthesized using previously described methods [38, 61].

[^{18}F]THK5317

In Papers IV-V, circa 3 MBq/kg [^{18}F]THK5317 was administered to the subjects at the start of the scan. Nine AD patients, four MCI patients and nine HC received a 90 min dynamic PET scan (25 frames; 6 × 10, 3 × 20, 2 × 30, 2 × 60, 2 × 150, 4 × 300 and 6 × 600 s) while remaining subjects received a 60 min scan (22 frames; 6 × 10, 3 × 20, 2 × 30, 2 × 60, 2 × 150, 4 × 300 and 3 × 600 s). The radiosynthesis of [^{18}F]THK5317 are described in the supplementary material of Paper IV.

Blood sampling

All subjects in Paper IV underwent arterial blood sampling during the [^{18}F]THK5317 PET scan. Discrete arterial blood samples were used for metabolite analysis and for measurement of whole-blood and plasma radioactivity to be applied as an input function in the analysis. Blood was drawn continuously during the first 10 min of the scan (3 mL/min) and discrete blood samples (5 mL) were taken at 5, 10, 15, 20, 30, 45, 60, 75 and 90 min p.i.

Image analysis

Image processing and VOI definition

All PET data were realigned to correct for subject movement using a rigid frame-to-frame realignment procedure in VOIager (GE Healthcare, Uppsala, Sweden). The MRI scans were co-registered to the first part of their respective [^{11}C]PE2I or [^{18}F]THK5317 PET images, 0-3 min and 0-5 min respectively, and segmented into grey matter, white matter and cerebrospinal fluid (CSF), using Statistic parametric imaging (SPM5 or SPM8; Wellcome Trust Center for Neuroimaging, University College London, UK). Volumes of interest were defined on the co-registered MRI images using a probabilistic VOI template implemented in the PVElab software [62]. Figure 7 shows the PVELab-obtained VOIs from one HC. In Paper II, the [^{18}F]FDG scans were summed

over all frames, and the [^{123}I]FP-CIT SPECT data were analysed by an automated VOI template [63] using the BRASS software (Hermes Medical Solution).

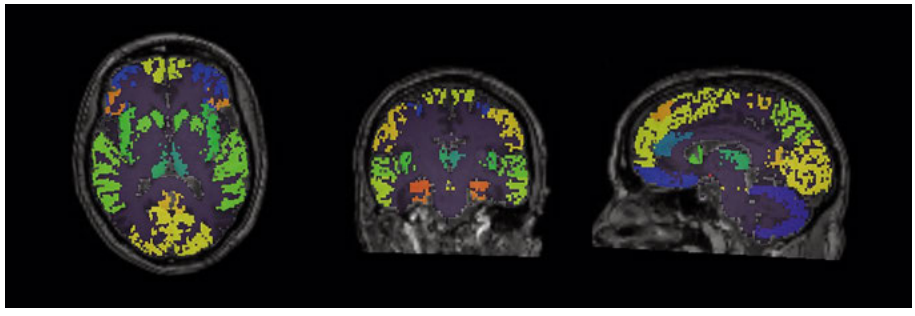

Figure 7. Example of PVElab VOIs from one healthy control fused with the subjects' MRI image. Different VOIs are shown in different colors.

Tracer kinetic analysis

Plasma input models

In order to obtain a plasma input function for the subjects in Paper IV, where blood sampling had been performed, the measured whole-blood data was multiplied by a single exponential fit to plasma–to–whole-blood ratios and a sigmoid fit to the measured fraction of intact [^{18}F]THK5317 in plasma. 1TCM and 2TCM were applied to the [^{18}F]THK5317 data in Paper IV, using the plasma input function. BP_{ND} values were calculated both directly and indirectly as DVR-1 and DVR-1 was also computed using plasma-input Logan.

Reference tissue models

SRTM was used for VOI-based analysis of [^{11}C]PE2I in Paper I, calculating both BP_{ND} and R_1, which in previous studies has shown a good correlation with compartmental modelling using plasma input [37, 45]. VOI-based analysis with SRTM was also performed for [^{18}F]THK5317, including the calculated BP_{ND} values in Paper IV and the R_1 values in Paper V. In both Paper IV and V, DVR-1 values were estimated for [^{18}F]THK5317 on a VOI-basis using reference Logan. For the reference region methods, grey matter cerebellum was considered the standard reference region for both [^{11}C]PE2I and [^{18}F]THK5317, since it is a region with no concentration of both DAT [61] and tau.

Parametric images

Voxel-wise analysis was performed for all [^{11}C]PE2I and [^{18}F]THK5317 data included in this thesis. First, in order to validate the models for generation of

parametric [^{11}C]PE2I BP_{ND} and R_1 images in Paper I, two basis function methods (RPM and RPM2) and three multilinear reference tissue models (MRTM, MRTMo and MRTM2) were applied. Additionally, DVR-1 images were generated using reference Logan using a time interval of 30-80 min, and SUVR-1 was estimated for each voxel for the last 20 min of the scan, 60-80 min. Voxel-level analysis of [^{18}F]THK5317, in Paper IV was performed using RPM and RPM2 for generation of parametric BP_{ND} images. Reference Logan DVR-1 images were generated on a time interval of 30-90 min and SUVR-1 images were estimated at 70-90 min.

Furthermore, RPM was used to generate BP_{ND} and R_1 images for [^{11}C]PE2I in Paper II and III, for both quantitative and visual comparison to [^{123}I]FP-CIT and [^{18}F]FDG images, respectively, and for comparison to the simplified analysis methods implemented in Paper III. In Paper V, parametric DVR-1 images of [^{18}F]THK5317 were generated using reference Logan and R_1 images was calculated with RPM.

In Paper II, the [^{18}F]FDG volumes were co-registered to the [^{11}C]PE2I R_1 image of the respective subject, in order to be able to apply the same set of VOIs to both images. The summed [^{18}F]FDG images were then normalized to cerebellum to obtain uptake ratio images.

Simulations

Simulations were performed in Paper I and IV to assess accuracy and precision of the models. Time-activity curves were simulated using 2TCM with a plasma input curve. The kinetic parameters were based on typical values from the literature for [^{11}C]PE2I [39, 45] in Paper I and with typical values from the clinical data for [^{18}F]THK5317, in Paper IV, and a plasma input function from one typical subject. For each set of parameters, 100 TACs were created and Gaussian noise was added randomly. The noise level was set to 2% to resemble the noise of a typical striatum- or cortical-VOI for [^{11}C]PE2I and [^{18}F]THK5317 respectively and to 10% to resemble the noise of a typical [^{11}C]PE2I striatal-voxel. Two set of rate constants were used for both [^{11}C]PE2I and [^{18}F]THK5317, to reflect both high and low binding.

Shorter acquisition time

Different durations of the acquired PET data were considered in order to evaluate the possibility of a shortened scan protocol. For [^{11}C]PE2I, the first 20 min (10 frames), 30 min (12 frames) and 40 min (14 frames) of the original 80 min data were considered in Paper III, as shown in Figure 8. DAT availability was approximated as SUVR-1 for the last two frames of each data set (14-20 min, 20-30 min and 30-40 min). In addition, parametric R_1 images were generated for each shortened data set using RPM.

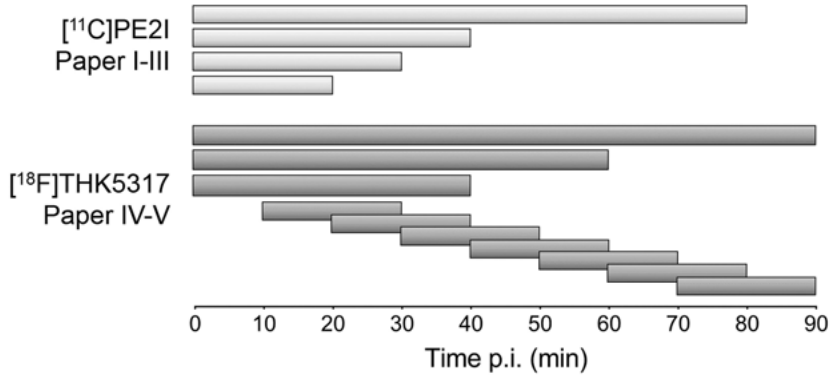

Figure 8. Schematic overview of the different durations of the acquired [^{11}C]PE2I and [^{18}F]THK5317 PET data considered for analysis.

For [^{18}F]THK5317, the initial 40 min (20 frames) and 60 min (22 frames) were evaluated in addition to the full 90 min data in Paper IV. For the shortened data sets, plasma-input Logan and reference Logan analysis were performed at a time interval of 20–40 min and 30–60 min, and SUVR-1 were calculated for 20–40 min and 40–60 min. The optimal timing of the SUVR measurements of [^{18}F]THK5317 was investigated in Paper V. The time at which TE occurred was determined as the peak of the specific binding curve for each considered VOI, calculated by subtraction of the grey matter cerebellum TAC from the VOI TAC. SUVR-1 was calculated for a 20 min interval centred around TE as well as for seven consecutive 20 intervals between 10 and 90 min p.i., see Figure 8.

Supervised cluster analysis

Although the principles of an implementation of the SVCA algorithm are similar for each tracer, this method needs to be validated for both [^{11}C]PE2I and [^{18}F]THK5317. An SVCA algorithm specific for [^{11}C]PE2I and [^{18}F]THK5317 was developed in Papers III and V. A set of kinetic classes was predefined on the dynamic PET data from the set of subjects that were included specifically for this purpose. Different regions were used for the definition of kinetic classes for [^{11}C]PE2I and [^{18}F]THK5317, but common for both tracers were the use of a grey matter cerebellum VOI as a class corresponding to non-specific binding. The definition of the classes other than grey matter cerebellum was aimed at avoiding inclusion of their associated voxels in the cerebellum class. The TACs from each kinetic class were normalized to their respective area under the curve. In order to generate reference TACs from the subjects included in the analysis, the TAC of each voxel in the dynamic data sets was also normalized to its area under the curve and a non-

negative least-squares algorithm was used to find a linear combination of the probability for each voxel to correspond to each kinetic class. Voxels with a probability higher than a specific limit, investigated for each tracer separately as described in Paper III and V, were assigned to that specific class. The voxels selected for the cerebellum class were regarded as reference region and a mean of the TACs of the selected voxels was calculated. The SVCA-extracted reference TAC was then used as input function to generate new parametric images for [^{11}C]PE2I and [^{18}F]THK5317.

[^{11}C]PE2I

In Paper III, five HC subjects were included for the predefinition of five kinetic classes. Except for the grey matter cerebellum class, striatum (corresponding to high specific binding), white matter, blood and a class to collect remaining voxels were defined. The SVCA-extracted reference TAC was then used as input function to generate new parametric BP_{ND} and R_1 images for the full 80 min [^{11}C]PE2I data, as well as SUVR-1 and R_1 images for the shortened data sets in the 12 HC and 12 patients with parkinsonism that were included for the analysis.

[^{18}F]THK5317

In Paper V, a set of four kinetic classes was predefined on dynamic [^{18}F]THK5317 data from 4 AD patients and 4 HC. Except for the grey matter cerebellum class, grey matter, white matter and a blood pool class were defined. The cerebellum class was defined on the HC subjects, to ensure that only healthy tissue was included, while the grey matter, white matter and blood pool classes were defined on the AD patients. New parametric SUVR-1 images for the optimal time window as well as RPM R_1 images were generated with the SVCA extracted reference TAC as input function.

All modelling, simulations and SVCA analysis were implemented in Matlab (Mathworks Inc., Natick, MA, USA).

Data evaluation

For quantitative evaluation of the parametric methods, regionally averaged voxel values were retrieved by projecting the MRI based PVElab VOIs onto the parametric images. The VOIs considered were specific for each study. Correlation and agreement between the different methods were assessed using the square of the correlation coefficient (R^2) and slope of a linear or orthogonal regression analysis.

Paper I

Evaluation of the parametric methods for [^{11}C]PE2I in Paper I was performed by comparing regionally averaged BP_{ND}, DVR-1 and SUVR-1 values, as well as R_1 values, from the parametric images to VOI-based STRM values. Seven different VOIs were considered: putamen, caudate, thalamus, midbrain, hypothalamus, amygdala and hippocampus, averaged over left and right. Mean values of the within subject correlation and agreement in these seven VOIs were assessed for both BP_{ND} and R_1. BP_{ND} and R_1 values of the parametric methods and VOI-based SRTM were also compared across subjects in a striatal VOI (mean of caudate and putamen) and in thalamus. In the simulation study, performance of the parametric methods was assessed by calculating the bias and coefficient of variation (COV) for the BP_{ND} and R_1 estimates of the parametric models considered.

Paper II

For comparison of the DAT availability of [^{11}C]PE2I and [^{123}I]FP-CIT SPECT images, VOIs over caudate and putamen were considered. Regionally averaged voxel values from the [^{11}C]PE2I BP_{ND} images were retrieved using the PVElab VOIs while for [^{123}I]FP-CIT, regional uptake values were normalized to occipital cortex, and retrieved using an automated VOI template as implemented in the BRASS software (Hermes Medical Solution). For comparisons of [^{11}C]PE2I R_1 and normalized [^{18}F]FDG images, four different sets of VOIs were considered including anterior cortical regions (cingulate and frontal cortex), posterior cortical regions (occipital-, parietal and somatosensory-motor cortex), striatal region (putamen and caudate) and a limbic region (amygdala, hippocampus, hypothalamus and thalamus). The imaging data was evaluated visually by two blinded nuclear medicine specialists. The image-based diagnosis was based on DAT availability in the [^{11}C]PE2I BP_{ND} or [^{123}I]FP-CIT images, rated as normal or abnormal, and the overall brain functional activity using the [^{11}C]PE2I R_1 or [^{18}F]FDG images, based on specific pathological patterns for glucose metabolism a reported for various parkinsonian disorders [24, 25, 64]. The most probable type of parkinsonism was determined for the set of BP_{ND} and R_1 images and for the [^{18}F]FDG and [^{123}I]FP-CIT images separately.

Paper III

In Paper III, the regions considered for evaluation of [^{11}C]PE2I BP_{ND} were, as in Paper I and II, putamen and caudate. For R_1, three set of VOIs were considered; striatum (caudate, putamen), a cortical group (frontal-, parietal, occipital, somatosensory and motor cortex) and a limbic group (thalamus, hypothalamus and amygdala). SUVR-1 and R_1 values of the shortened data sets; 20,

30 and 40 min, were compared to the BP_{ND} and R_1 values of the complete 80 min data. BP_{ND} and R_1 values obtained using of the full 80 min [^{11}C]PE2I data with either an MRI-based or SVCA-based reference were compared. In the same way, SUVR-1 and R_1 values of the shortened data sets with SVCA-based reference were compared to the BP_{ND} and R_1 values with MRI-based reference. The standardized difference between the mean BP_{ND} and SUVR-1 values (Cohens d), between the HC and the subjects with parkinsonian disorders, was calculated for each scan duration and with both MRI- and SVCA-based reference.

Paper IV

Eleven VOIs were included in the evaluations of the tracer kinetic analysis of [^{18}F]THK5317; thalamus, putamen, hippocampus, amygdala, midbrain, parietal-, frontal-, temporal entorhinal- occipital- and sensory motor cortex, all averaged over left and right hemispheres. The optimal plasma-input compartment model was determine using Akaike [65] and Schwarz [66] criteria. Furthermore, VOI-based BP_{ND} and DVR-1 from the reference tissue models, SRTM and reference Logan, were compared to the optimal plasma input compartment model and plasma input Logan. The parametric methods were quantitatively evaluated by comparison to the VOI-based values from the optimal reference method. Bias and COV were calculated for the BP_{ND}, DVR-1and SUVR-1 estimates of the simulated [^{18}F]THK5317 data.

SRTM BP_{ND}, reference Logan DVR-1 and SUVR-1 of the shortened data sets, 40 and 60 min, were compared their respective binding estimates when using the full 90 min data.

Paper V

The relationship between SUVR-1 of the different time interval for the [^{18}F]THK5317 scan and reference Logan DVR-1 were assessed by correlation and bias analysis. SUVR-1 values at the optimal time interval calculated with SVCA-based reference were compared to those using an MRI-based reference region. Parametric RPM R_1 values of the shortened scan duration, matching that of the optimal time found for SUVR-1 estimations, were compared to SRTM R_1.

Results

[^{11}C]PE2I

Parametric images

For [^{11}C]PE2I, the results of Paper I showed that the receptor parametric methods, RPM and RPM2, provided qualitatively the best images for both the parkinsonism patients and SAD subjects, especially with regards to the R_1 images. None of the multi linear reference tissue models could provide qualitatively good images. The within-patient comparison of the parametric methods to VOI-based SRTM showed a high correlation for the BP_{ND} estimates for all methods, while only RPM- and RPM2-based R_1 values showed a high correlation to SRTM R_1 values. In the across-subject comparison in thalamus and striatum separately, RPM and RPM2 showed the highest correlation to SRTM, regarding both BP_{ND} and R_1. Both DVR-1 values obtained using reference Logan and SUVR-1 showed a high correlation to SRTM BP_{ND}, whereas SUVR-1 values were greatly overestimated as compared to BP_{ND}. Parametric RPM BP_{ND} and R_1 images are shown in Figure 9.

Simulations

The highest accuracy and precision of [^{11}C]PE2I BP_{ND} and R_1 estimates of the different parametric method was found for the receptor parametric mapping methods, with a better accuracy for RPM than RPM2, for both high and low BP_{ND} values.

Relationship between [^{11}C]PE2I and the dual scan approach

Comparison between [^{11}C]PE2I BP_{ND} and [^{123}I]FP-CIT uptake ratio values showed a high correlation in putamen, R^2=0.92 and a lower correlation in caudate, R^2=0.57. Relationship between the [^{11}C]PE2I R_1 and normalized [^{18}F]FDG values showed a variety of correlation values over different brain regions, ranging from R^2=0.37 – 0.88, with the lowest correlations in the midbrain and limbic regions and the highest correlations in the cortical regions.

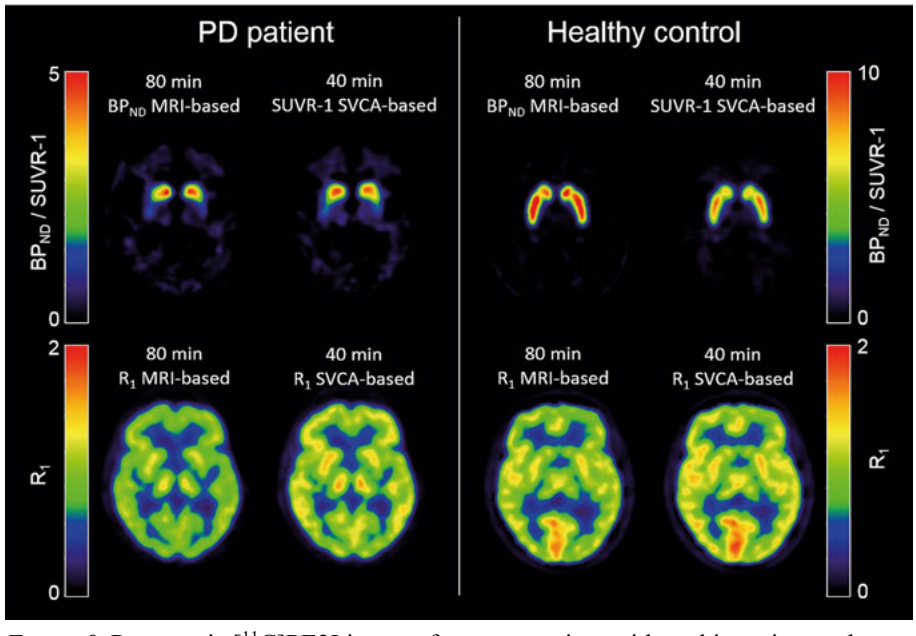

Figure 9. Parametric [^{11}C]PE2I images from one patient with parkinsonism and one HC. Top row comparing BP_{ND} and SUVR-1 and bottom row R_1 for different scan durations with either an MRI- or SVCA-based reference region.

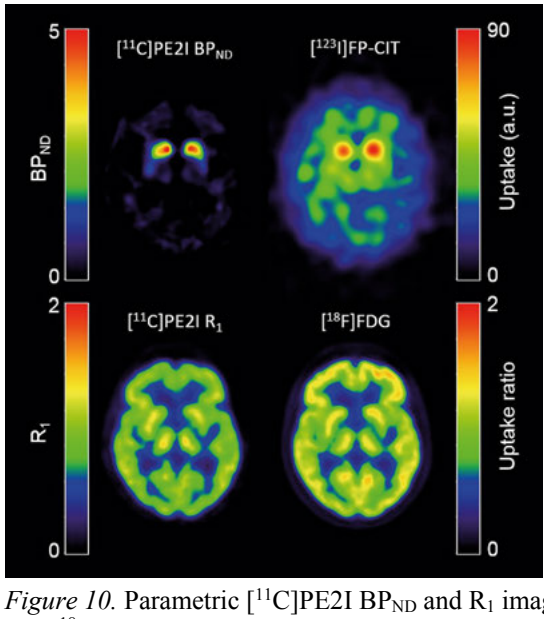

Figure 10. Parametric [^{11}C]PE2I BP_{ND} and R_1 images compared with [^{123}I]FP-CIT and [^{18}F]FDG images from one patient with parkinsonism.

Visual image assessment

Regarding the diagnosis of the patients, based on the visual image assessment of both DAT availability and overall brain function, there were 4 discrepancies between the two data sets of [^{11}C]PE2I R_1 and BP_{ND} or normalized [^{18}F]FDG and [^{123}I]FP-CIT uptake images. Discrepancies from the clinical diagnoses was found in 9 cases compared to parametric [^{11}C]PE2I images and in 8 cases compared to the dual scan approach. An example of a comparison between the [^{11}C]PE2I BP_{ND} and R_1 images and normalized [^{18}F]FDG and [^{123}I]FP-CIT uptake images is given in Figure 10.

Acquisition time

Striatal SUVR-1 calculated on time intervals of 20-30 and 30-40 min showed a high correlation to BP_{ND} values of the full 80 min scan (R^2=0.82 and 0.87, respectively), while correlation was lower for SUVR-1 at 14-20 min.

SUVR-1 values were underestimated compared to BP_{ND} values, with the underestimation increasing for decreasing scan time. R_1 values of the shortened data sets showed a high correlation to R_1 of the full 80 min data in all regions and for all scan durations. One subject was found to deviate in terms of high R_1 values. This outlier corresponds to a parkinsonism subject with probable MSA with cerebellar atrophy. The decreased blood flow in cerebellum of this subject (see Figure 3 in Paper II) resulted in excessively high R_1 values when using cerebellum as a reference region.

Supervised cluster analysis

The relationship between BP_{ND} using an MRI- and SVCA-based reference region at the full scan duration showed a high correlation, R^2=0.99. R_1 values computed with SVCA-based reference region also showed high correlations compared to an MRI-based reference. When comparing the parametric estimates of the shortened scan durations with SVCA-based reference to BP_{ND} and R_1 values of the full scan duration calculated using MRI-based reference, the correlation was high regarding striatal SUVR-1 estimates with SVCA-reference region for all scan durations, R^2>0.85. R_1 values calculated with SVCA-based reference showed a high correlation to MRI-based R_1 values for all scan duration, in both striatal and limbic regions (R^2=0.84-0.94), but with an overestimation compared to 80 min R_1 with MRI-based reference. A lower correlation was found between the R_1 values of the shortened scan durations and SVCA-based reference compared to 80 min R_1 with MRI-based reference in cortical regions. A comparison between 80 min BP_{ND} and R_1 images with MRI-based reference and 30-40 min SUVR-1 and 40 min R_1 images with SVCA-based reference are shown in Figure 9. BP_{ND} and SUVR-1 values in putamen for the two groups separately, is shown in Figure 11A, for all scan

durations using an SVCA-based reference, as well as for the full 80 min data using MRI-based reference. The effect size (Cohen's d) is shown in Figure 11B, with values ≥4 for all acquisition times with SVCA-based reference, indicating a high degree of discrimination between patients with parkinsonism and HCs.

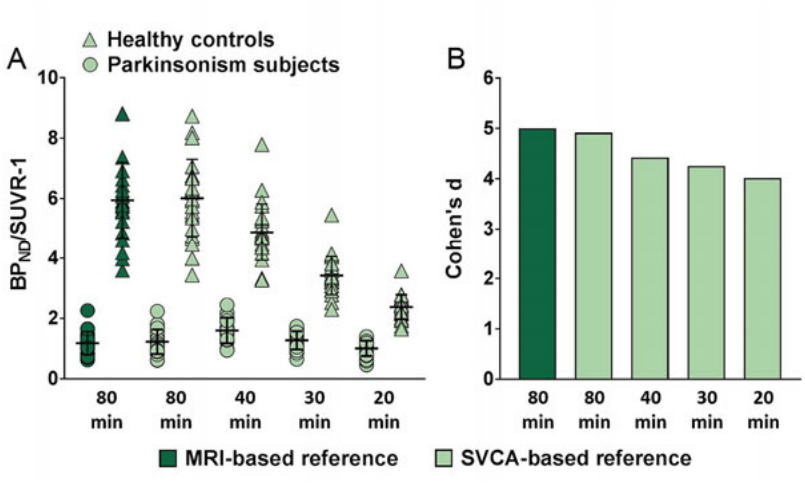

Figure 11. A) BP_{ND} values for the full 80 min acquisition time with both MRI- and SVCA-based reference region, and SUVR-1 values for the shorter scan durations with SVCA-based reference, in putamen, for the HCs and the patients with parkinsonism. Horizontal bars show mean and standard deviation of each group. B) Standardized difference of the mean (Cohen's d) of BP_{ND} and SUVR-1 values in putamen between the patients with parkinsonism and the HCs for varying scan durations

[^{18}F]THK5317

Tracer kinetic analysis

The 2TCM showed a better fit to the data than 1TCM and was also the preferred method according to both Akaike and Schwarz criteria in all cases except two. However, BP_{ND} was not possible to determine directly with any robustness using 2TCM. A high agreement between 2TCM DVR-1 and plasma-input Logan DVR-1 was found, and plasma-input Logan was used for evaluation of the reference methods. Both reference Logan DVR-1 and SRTM BP_{ND} showed high accuracy when compared to plasma input models, with R^2 and slope values close to, or equal to, one. SUVR-1 values for a late time window of 70-90 min showed a poor correlation and were overestimated compared to both plasma input Logan DVR-1 and SRTM BP_{ND}.

Parametric images

Three of the four methods used for generating parametric methods; RPM RPM2 and reference Logan, showed a very high correlation to VOI-based SRTM values, with $R^2 \geq 0.98$. However, the agreement, as indicated by the slope was best for reference Logan. SUVR-1 at 70-90 min was overestimated compared to the other methods and showed only moderate correlation to SRTM. Parametric reference Logan DVR-1 and RPM R_1 images are shown in Figure 12 for one AD and on HC.

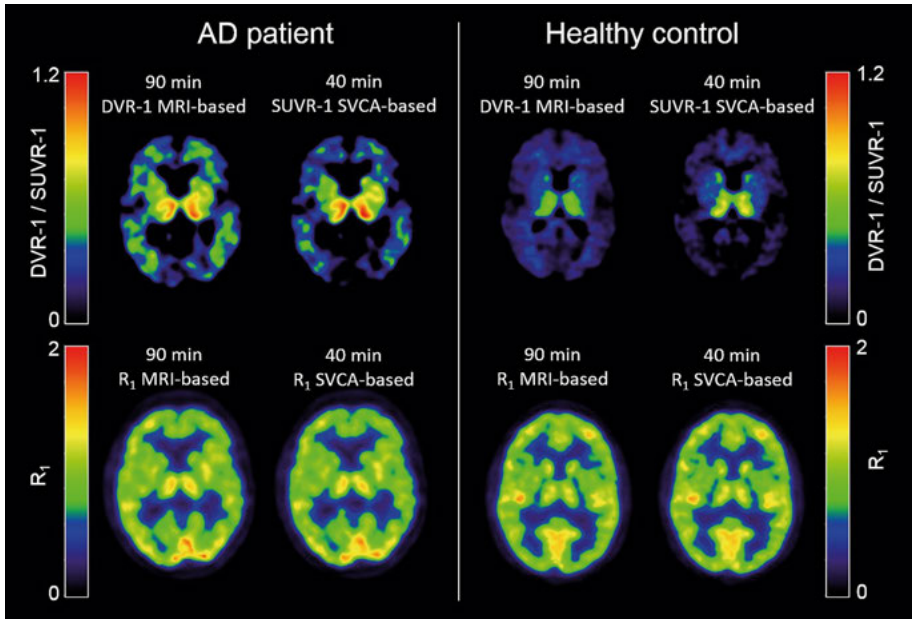

Figure 12. Parametric [^{18}F]THK5317 images from on AD patient and one HC. Top row comparing DVR-1 and SUVR-1 and bottom row R_1 for different scan durations with either an MRI- or SVCA-based reference region.

Simulations

Accuracy and precision of the simulated BP_{ND}, DVR-1 and SUVR-1 values for the different methods were in general better for low binding than for high binding. Reference Logan performed best among the reference methods and showed a lower COV than plasma input Logan.SUVR-1 was the least accurate for both high and low binding.

Acquisition time

There was no appreciable effect on SRTM BP_{ND} and reference Logan DVR-1 when decreasing the scan duration to 60 min, while the correlation was poorer with the 40 min data set. SUVR-1 at 20-40 min values were underestimated

compared to the 70-90 min interval. Time to TE varied across regions, which is shown in Figure 13A, but over all subjects and regions, SUVR-1 for a 20-40 min time window correlated best with reference Logan DVR-1, and showed the lowest mean bias. Cohen's d between AD patients and HCs of DVR-1 and SUVR-1 at TE and the different time intervals, for amygdala, parietal-, temporal- and entorhinal cortex are shown in Figure 13B.

Supervised cluster analysis

High correlation was found both between SUVR-1 for an 20-40 min time window, with MRI- and SVCA-based reference (R^2=0.93) and between 40 min R_1 values with SVCA-based reference and 90 min R_1 values with MRI-based reference (R^2=0.94). A comparison between reference Logan DVR-1 and R_1 images with MRI-based reference and 20-40 min SUVR-1 and 40 min R_1 images with SVCA-based reference is shown in Figure 12. Highest Cohen's d values were found for parietal cortex for time windows centred around 30 min and higher.

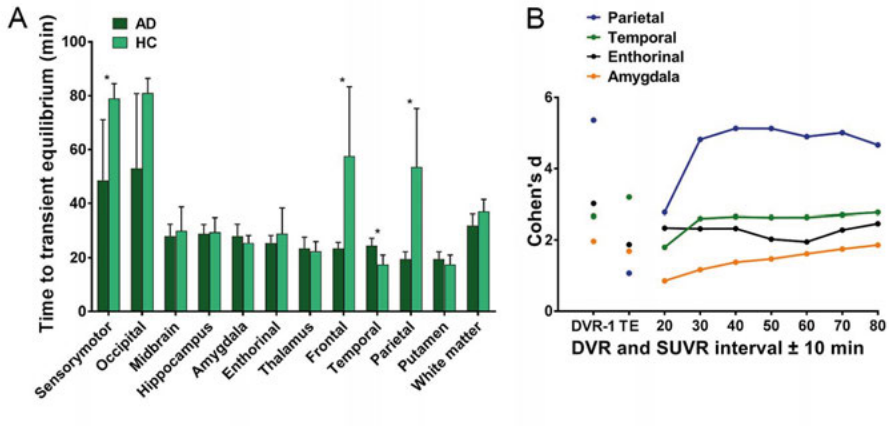

Figure 13. A) Mean time to TE for the investigated regions. B) Cohen's d as a function of DVR-1 and SUVR-1 at TE and the different time intervals, between AD patients and HCs.

Discussion

[^{11}C]PE2I

The first step in this thesis was to validate parametric methods for voxel-wise quantification of [^{11}C]PE2I. The results in Paper I showed that the receptor parametric mapping methods, RPM and RPM2, showed robust and quantitatively correct results, both for clinical data and simulated data. Previous studies have shown an underestimation of 30-50% for BP_{ND} in DAT rich regions when using a reference region method compared to plasma-input models [38, 39]. It has been discussed previously that the kinetics of the cerebellum may be affected by possible uptake of metabolites retaining the ^{11}C label. In this case, the reference tissue methods will show an underestimation compared to BP_{ND} estimated using plasma-input method. However, if metabolites are not binding specifically, and their uptake is uniform across brain regions, this should not affect correlation between plasma- and reference-tissue-based BP_{ND} estimates. The importance of an underestimation of BP_{ND} is small as long as there is a good correlation between the estimates obtained from the reference tissue and plasma input model [67].

The results from Paper II shows that [^{11}C]PE2I BP_{ND} and R_1 images comprised information equivalent to the dual scan approach with [^{123}I]FP-CIT SPECT and [^{18}F]FDG PET scans, in terms of specific pathologic patterns and correlations of quantitative values. In about half of the patients, the clinical diagnosis deviated from the imaging results. A previous study has reported similar results, with more than 50% of the initial clinical diagnosis changed after imaging with [^{123}I]FP-CIT SPECT [68]. To date, no long-term follow-up is available to assess the correctness of the image-based diagnosis for the included patients.

The major challenge for clinical use of [^{11}C]PE2I is the long scan acquisition time required which is not suitable in a clinical setting and especially not for patients suffering from movement disorders, as well as the need for an additional structural MRI scan for reference region definition. These issues were addressed in Paper III, where a clinically feasible scan protocol and analysis methods were evaluated. For the shorter scan duration, the DAT availability was estimated as SUVR-1, with the time window of 30-40 min showing the highest correlation the 80 min BP_{ND} values. For [^{11}C]PE2I, TE occurs at around 30 min which further supports use of the 30-40 min time interval for SUVR estimations.

Irrespective of the use of an MRI- or SVCA-based reference region, SUVR-1 values for scan durations shorter than 40 min showed a low correlation and agreement to the 80 min BP_{ND} values, and a lower difference between SUVR-1 of the group of parkinsonism patients and the control group.

The shorter scan durations did not to any major extent affect the accuracy of R_1 values as long as an MRI-based reference region was used. A lower correlation to R_1 values for the original 80 min data with an SVCA-based reference was however observed in cortex R_1. One reason for this may be the relatively narrow range of cortical R_1 values. However, the within-subject correlation between the R_1 values of the based on an SVCA reference region and the 80 min R_1 values with MRI-based reference was high for all scan durations.

A limitation in the study in Paper III is the significantly higher age of the patients then of the controls. Previous PET studies have reported an age-related decline of DAT in both caudate and putamen of 6 -8 % per decade [69, 70]. This suggests that the different between the two groups in Paper III would have been lower if they had been of the same age. Recently, we investigated the age related-effect of DAT availability measured with [^{11}C]PE2I, using both BP_{ND} and SUVR-1 measures and using the methods presented in this thesis. In line with a previous study with [^{18}F]FE-PE2I, there was a mean decline of 7.6% and 6.2% per decade of BP_{ND} and SUVR-1, respectively, in caudate. However, no significant decline of either BP_{ND} or SUVR-1 was observed in putamen, see Appendix A. These results, deviating from previous studies, need to be further investigated. Thus, while using the same analysis methods as implemented for [^{11}C]PE2I analysis in Paper III, these findings indicates that there would be no further decrease of the difference between the two groups in putamen, regardless of using age-matched controls. However, for clinical assessment of DAT availability, the age-related decline needs to be considered for both BP_{ND} and SUVR-1 values in caudate.

Another challenge for the clinical application of [^{11}C]PE2I, is the short half-life of ^{11}C, 20.4 min. This requires access to a cyclotron and on-site tracer production, in contrast to for example [^{123}I]FP-CIT or ^{18}F-labelled DAT ligands such as [^{18}F]FE-PE2I. However, in generally, the differential diagnosis of parkinsonism takes place at specialized hospitals that often have access to a tracer production facility.

Advantages of using [^{11}C]PE2I PET over [^{123}I]FP-CIT are the higher resolution of PET compared to SPECT as well as the inherently quantitative nature of PET, which is further utilized by generating parametric images. [^{11}C]PE2I also has a higher selectivity to DAT than [^{123}I]FP-CIT, which also binds to serotonin and norepinephrine transporters [71]. In addition, there is a reduction of the radiation dose of about 70% when using a single [^{11}C]PE2I PET scan compared to the dual scan approach with both [^{123}I]FP-CIT and [^{18}F]FDG, and the need for a single hospital visit only, to assess both DAT availability and overall brain functional activity.

[^{18}F]THK5317

The results from Paper IV showed that the [^{18}F]THK5317 kinetics were best described applying the 2TCM, with tau binding estimated as DVR-1. Both SRTM BP_{ND} and reference Logan DVR-1 agreed well with plasma-input models. Reference Logan DVR-1 performed best when applied on a voxel-level and agreed best to VOI-based SRTM values. The evaluation of shorter scan durations in Paper IV showed that 60 min was sufficient for accurate quantification using reference Logan DVR-1 measures. The results from Paper V demonstrated that the scan duration could be further decreased when estimating [^{18}F]THK5317 binding using SUVR-1. There was a high variation of time to TE across the different brain regions, and between AD and HC, which complicates the definition of a general time interval for SUVR-1 calculations. However, SUVR-1 for the 20-40 min time interval showed highest correlation and agreement to the DVR-1 values overall, for both AD and HC subjects.

As shown in Paper IV, there is a high white matter uptake primarily because of the lower clearance rate in white matter than in grey matter regions. The parametric BP_{ND} or DVR-1 images considerably reduced the high with matter signal as compared with SUVR-1 at 70-90 min. Partial volume corrections were not assessed in this work but could possibly improve the quantitative accuracy by accounting for white-matter spill-over.

SUVR-1 at the time interval of 20-40 min using an SVCA-based reference showed a high agreement to SUVR-1 with MRI-based reference indicating that the SVCA method can be used to provide a reference TAC directly from the dynamic [^{18}F]THK5317 scan.

As previously shown, R_1 estimate from the dynamic [^{18}F]THK5317 scan demonstrates a high correlation to [^{18}F]FDG uptake [72] and as shown here, a 40 min scan duration is sufficient for measuring R_1 with an SVCA-based reference. This makes it possible to use dynamic [^{18}F]THK5317 for dual-biomarker investigations and could potentially serve as a substitute for [^{18}F]FDG.

There has been some concern about binding of tau tracers such as the structurally related tracer [^{18}F]THK5351 to monoamine oxidase-B (MAO-B) present in astrocytes [73]. A recent in vitro study of the racemic compound [^{3}H]THK5117 showed relatively low affinity to monoamine oxidase-B indicating that competitive binding of the corresponding [^{18}F]THK5317 would not present a problem at the concentrations encountered during clinical PET studies [74, 75], although *in vivo*, an off target binding is evident in the basal ganglia [76]. However, newly developed tau tracers that are being evaluated, such as [^{18}F]MK6240, are showing much lower off-target binding [77, 78].

General discussion

The use of short, static scans is attractive for clinical applications. A dynamic PET scan can however result in parametric images showing both the binding of the tracer and also the relative tracer delivery, which can be used for assessment of overall brain function. Using simplified analysis methods and decreased scan duration, while maintaining quantitative accuracy, can facilitate the use of dynamic PET in clinical practice as well as in research investigations.

Even though an MRI in many cases is performed in patients with neurodegenerative disease, an automated way of extracting the reference region can still be of value to simplify the analysis of dynamic PET data. In some cases, as seen for example in the MCI subject with degeneration of cerebellum, in Paper III, the use of an SVCA-based reference provided more correct quantification than when cerebellum was used as reference. This may also apply to other types of brain injuries with associated tau pathology, as for example brain trauma patients where the cerebellum can be impaired.

The results in this work are not directly applicable to other PET tracers. Issues such as differing kinetics may influence the choice of cluster classes for implementation of SVCA and an optimal time window for calculations of semi-quantitative values, such as SUVR-1, should be evaluated carefully for each tracer. However, the underlying methods evaluated in this thesis can be useful for many different applications.

Concluding remarks

The overall focus of this thesis has been to evaluate models for quantification of dynamic [^{11}C]PE2I and [^{18}F]THK5317 PET data, and to validate simplifications of these methods, suitable for use in a clinical setting.

[^{11}C]PE2I

Papers I-III supply valuable information on the feasibility of the clinical use of dynamic [^{11}C]PE2I for differential diagnosis of parkinsonian disorder. The main findings in Papers I-III were the following:

I Parametric [^{11}C]PE2I images showing DAT availability, BP_{ND}, and the relative tracer delivery, R_1, can be robustly obtained using RPM.

II The parametric BP_{ND} and R_1 images from a single dynamic [^{11}C]PE2I scan can be used to evaluate parkinsonian disorders and their use is a powerful alternative to a dual scan approaches with [^{123}I]FP-CIT and [^{18}F]FDG.

III Simplification of the acquisition and analysis methods for [^{11}C]PE2I is possible by shortening the scan acquisition time to 40 min and using a clustering method to obtain a reference region directly from the dynamic scan, while still adequately being able to discriminate between control subjects and patients with reduced DAT availability.

In 2015, [^{11}C]PE2I was introduced clinically at Uppsala University Hospital and in 2017 over 120 patients with parkinsonian disorders have been investigated with [^{11}C]PE2I and the methods developed in this thesis.

[^{18}F]THK5317

The work in Papers IV-V showed that simplified analysis methods can be applied for quantification of [^{18}F]THK5317 and the main findings were the following:

I A reference tissue method can be used for quantification of tau pathology with [^{18}F]THK5317 on both VOI- and voxel-level, overcoming the need for arterial blood sampling.

II An SVCA-based reference region combined with a scan duration of 40 min, for assessment of both SUVR-1 and R_1 measures, can be applied to further exploit applications of [^{18}F]THK5317 PET.

Future perspectives

The methods developed and validated in this thesis have shown great potential for clinical applications. Although these results are not directly applicable to other PET tracers, evaluation of these methods for quantification of dynamic PET data using other tracers could possibly further facilitate use of dynamic, multi-parameter PET in clinical settings.

For example, as mentioned in the discussion, the use of [^{11}C]PE2I is limited to hospitals with access to a cyclotron and tracer production facilities. Therefore, implementation of these methods for a ^{18}F-labelled tracer such as [^{18}F]FE-PE2I would make the methods described for [^{11}C]PE2I available outside of the university hospitals. This could also enable multi-centre research collaborations to increase the knowledge of Parkinson's disease and similar syndromes.

The use of a supervised clustering method could also be of great potential when investigating diseases where the cerebellum may be affected and implementation of SVCA could be a strategy for accurate quantification of dynamic PET data these patients.

Summary in Swedish

Positronemissionstomografi (PET) är en funktionell avbildningsmetod som bygger på att en spårsubstans märkt med en radioaktiv isotop, till exempel kol-11 (^{11}C) eller fluor-18 (^{18}F), administreras i kroppen. Den strålning som spårsubstansen ger upphov till kan registreras av PET-kameran och distributionen av spårsubstansen i kroppen kan mätas. Genom att göra PET-mätningen över tid, en så kallad dynamisk undersökning, fås information om hur koncentrationen av spårämnet i kroppen förändras över tid. Med den informationen, och med hjälp av olika matematiska modeller, kan kvantitativa parametrar som till exempel relativa blodflödet och bindning av spårsubstansen till specifika mål i kroppen, beräknas. Dessa beräkningar kan göras för varje pixel i PET-bilden, så kallade parametriska bilder, vilket ger en tydlig visuell uppskattning av de parametrar som är av intresse. På detta sätt kan alltså mycket mer information fås från en PET-undersökning än om man bara en statisk bild hade tagits, men det kräver vanligtvis en längre undersökningstid (60-90 min istället för 10-20 min) och i vissa fall samtidig blodprovstagning, vilket gör undersökningen svår för patienterna.

Alzheimers sjukdom och Parkinsons sjukdom är de två vanligaste neurodegenerative sjukdomarna i världen. Vid Parkinsons sjukdom och andra parkinsonliknande tillstånd är hjärnans dopaminsystem och övergripande funktion förändrad i olika grad. Gemensamt för dessa sjukdomar är att det kan varas svårt att erhålla en entydig diagnos utifrån enbart kliniska undersökningar. Med hjälp av PET och spårämnet [^{11}C]PE2I så kan tillgängligheten av dopamintransportörer (DAT) i hjärnan mätas. Hos patienter med parkinsonism föreligger det vanligtvis en nedsatt DAT-tillgänglighet. Alzheimers sjukdom karaktäriseras av en mängd olika komplexa patofysiologiska processer. En av dessa är ackumulering av proteinet tau i hjärnan, vilket är nära länkat till neurodegeneration och försämrad kognitiv förmåga. PET och spårämnet [^{18}F]THK5317 kan mäta tillgänglighet av tau-protein in hjärnan, som är en tidig markör för Alzheimers sjukdom.

PET kan spåra relativt små biologiska förändringar i hjärnans funktion och kan var till stor nytta både vid forskningsstudier och vid klinisk utvärdering av dessa sjukdomar. För att beräkna parameterbilderna från dynamiska PET-undersökningar utan att behöva ta blodprover krävs att det går att definiera en region i hjärnan som inte har någon bindning av spårsubstansen, en så kallad referensregion. Detta görs vanligtvis manuellt eller med automatiska metoder som kräver att man har tillgång till en strukturell bild av patientens hjärna, tex

från en magnetresonanstomografi (MRT) undersökning. För att förenkla användningen av dynamisk PET är det önskvärt att de relativt långa undersökningstiderna kan förkortas och att det går att använda förenklade analysmetoderna för kvantifiering av de parametrar som är av intresse samt att kunna definiera en referens-region direkt från det dynamiska PET-datat.

Syftet med den här avhandlingen var dels att utvärdera metoder för att ta fram kvantitativa mått för både bindningen och relativa flödet från dessa PET-undersökningar och att validera förenklade analysmetoder. Förkortade undersökningstider och automatiserade sätt att ta fram den referensregion som krävs för att kunna beräkna parameterbilderna för både [^{11}C]PE2I och [^{18}F]THK5317 data undersöktes också. Dessutom jämfördes bilder av DAT-tillgängligheten och relativa blodflödet, som beräknats från en [^{11}C]PE2I undersökning, mot tidigare bilddiagnostiska metoder för differentialdiagnostik av parkinsonism, som har krävt två separata undersökningar. Både friska kontroller och patienter med parkinsonism och Alzheimers sjukdom inkluderades för PET-undersökningarna.

Resultaten från de ingående arbetena i avhandlingen har visat att de parameterbilder som tagits fram från en dynamisk [^{11}C]PE2I PET undersökning i hög grad överensstämmer med de upptagsmönster som man ser vid de tidigare undersökningsmetoderna. Det har också visats att det är möjligt att korta ner den dynamiska PET-undersökningen från 80 till 40 min och fortfarande behålla den kvantitativa informationen avseende DAT-tillgänglighet och relativt blodflöde. Dessutom kan en klustermetod användas för att ta fram en referensregionen direkt från den dynamiska PET undersökningen, vilket ytterligare förenklar analysen av bilderna. Liknande resultat sågs för [^{18}F]THK5317, där både reducerad undersökningstid, från 90 till 40 min, och förenklade analysmetoder för kvantifiering av tau-bindning och relativt blodflöde kan användas för att dra nytta av dynamisk [^{18}F]THK5317 PET.

Metoderna som har utvecklats i denna avhandling gör det möjligt att till fullo använda de möjligheter PET ger när det gäller att mäta flera olika processer i hjärnan under en och samma undersökning, med en undersökningstid som är tillräckligt kort för att kunna användas i kliniken och med nästan helt automatiskt bildanalys. Sedan 2015 har [^{11}C]PE2I, och de metoder som utvecklats och validerats i den här avhandlingen, använts kliniskt på Akademiska sjukhuset i Uppsala för differentialdiagnostik av patienter med parkinsonism.

Acknowledgments

The work to finalize this thesis would not have been possible without collaborations and the support by many. I would like to specially thank a few people:

First of all, my main supervisor, Mark Lubberink. I am so grateful that you took me on as a PhD student, for having the opportunity to learn from you and to work with you. Thank you for your patience, your enthusiasm and for believing in me. My co-supervisors; Lieuwe Appel, for interesting discussions and all the time you spent to thoroughly improving my manuscripts and Jens Sörensen, for your great expertise and valuable scientific input.

Everyone, past and present, at *'våning 5'* for making the work environment more enjoyable. Especially Ezgi, Kerstin, Camilla, Elin, Naresh and Joao, for being a part of this journey, for being great room-mates and friends and for cheering me up through times of stolen computers and broken hard drives. I want to thank all my past and present colleagues at the PET centre and medical physics at Uppsala University Hospital, especially Anders Wall, Torsten Danfors, Charles Widström and Jonas Eriksson for valuable scientific (as well as non-scientific) discussions and Lars Lindsjö and Tomas Nyholm for assistance with data handling.

The group of psychologists that I have had the opportunity to collaborate with from the start; Andreas Frick, Jonas Engman, Tomas Furmark and Mats Fredrikson. Thank you for always being super optimistic and for providing me with a lot of data.

I want to thank Dag Nyholm and Håkan Askmark for collaboration in the [^{11}C]PE2I project and for inclusion of the patients with parkinsonism.

Thanks to Agneta Nordberg for the possibility to work with the [^{18}F]THK5317 data and for the interesting collaboration with your group, including Konstantinos Chiotis, Laure Saint-Aubert and Antoine Leuzy, at the Center for Alzheimer Research at Karolinska Institutet. Thanks for sharing your knowledge in the field of PET in Alzheimer's disease.

All co-authors not already mentioned; Gunnar Antoni, Helena Wilking, Margareta Sprycha, Beatrice Borg and Alf Thibblin. I want to thank everyone that has contributed to the papers in this thesis with invaluable feedback and great input. I also want to take the opportunity to thank all research participants, without whom these studies would not have been possible.

My friends and family that have supported me on this journey. Especially Josse and Chris for always believing in me, even though you had no clue what I was doing ;-). Emma and Daniel for all the ‘fredagsmys’, I would not have stayed sane without it. My mother Eva and father Arnold, thank you for always telling me that it is fun to learn new thing. My siblings with families and Janne and Ingrid.

And finally, Patric, for your endless love and support, and Milo, for giving everything a new meaning. I dedicate this thesis to you!

References

1. Cherry S.R., S.J.A., Phelps M.E., *Physics in Nuclear Medicine*. 3rd ed. 2003, Philadelphia: Saunders.
2. Mintun, M.A., et al., *A quantitative model for the in vivo assessment of drug binding sites with positron emission tomography.* Ann Neurol, 1984. **15**(3): p. 217-27.
3. Logan, J., et al., *Graphical analysis of reversible radioligand binding from time-activity measurements applied to [N-11C-methyl]-(-)-cocaine PET studies in human subjects.* J Cereb Blood Flow Metab, 1990. **10**(5): p. 740-7.
4. Lammertsma, A.A. and S.P. Hume, *Simplified reference tissue model for PET receptor studies.* Neuroimage, 1996. **4**(3 Pt 1): p. 153-8.
5. Wu, Y. and R.E. Carson, *Noise reduction in the simplified reference tissue model for neuroreceptor functional imaging.* J Cereb Blood Flow Metab, 2002. **22**(12): p. 1440-52.
6. Gunn, R.N., et al., *Parametric imaging of ligand-receptor binding in PET using a simplified reference region model.* Neuroimage, 1997. **6**(4): p. 279-87.
7. Logan, J., et al., *Distribution volume ratios without blood sampling from graphical analysis of PET data.* J Cereb Blood Flow Metab, 1996. **16**(5): p. 834-40.
8. Ichise, M., et al., *Noninvasive quantification of dopamine D2 receptors with iodine-123-IBF SPECT.* J Nucl Med, 1996. **37**(3): p. 513-20.
9. Ichise, M., et al., *Linearized reference tissue parametric imaging methods: application to [11C]DASB positron emission tomography studies of the serotonin transporter in human brain.* J Cereb Blood Flow Metab, 2003. **23**(9): p. 1096-112.
10. Turkheimer, F.E., et al., *Reference and target region modeling of [11C]-(R)-PK11195 brain studies.* J Nucl Med, 2007. **48**(1): p. 158-67.
11. Yaqub, M., et al., *Optimization of supervised cluster analysis for extracting reference tissue input curves in (R)-[(11)C]PK11195 brain PET studies.* J Cereb Blood Flow Metab, 2012. **32**(8): p. 1600-8.
12. Ikoma, Y., et al., *Reference region automatic extraction in dynamic [(11)C]PIB.* J Cereb Blood Flow Metab, 2013. **33**(11): p. 1725-31.

13. Lyoo, C.H., et al., *Image-derived input function derived from a supervised clustering algorithm: methodology and validation in a clinical protocol using [11C](R)-rolipram.* PLoS One, 2014. **9**(2): p. e89101.
14. Rissanen, E., et al., *Automated reference region extraction and population-based input function for brain [(11)C]TMSX PET image analyses.* J Cereb Blood Flow Metab, 2015. **35**(1): p. 157-65.
15. Meyer, P.T., et al., *Dual-biomarker imaging of regional cerebral amyloid load and neuronal activity in dementia with PET and 11C-labeled Pittsburgh compound B.* J Nucl Med, 2011. **52**(3): p. 393-400.
16. Forsberg, A., et al., *The use of PIB-PET as a dual pathological and functional biomarker in AD.* Biochim Biophys Acta, 2012. **1822**(3): p. 380-5.
17. Ito, H., et al., *Comparison of the transient equilibrium and continuous infusion method for quantitative PET analysis of [11C]raclopride binding.* J Cereb Blood Flow Metab, 1998. **18**(9): p. 941-50.
18. Heurling, K., et al., *Quantitative positron emission tomography in brain research.* Brain Res, 2017. **1670**: p. 220-234.
19. Chaudhuri, K.R., D.G. Healy, and A.H. Schapira, *Non-motor symptoms of Parkinson's disease: diagnosis and management.* Lancet Neurol, 2006. **5**(3): p. 235-45.
20. Adler, C.H., et al., *Low clinical diagnostic accuracy of early vs advanced Parkinson disease: clinicopathologic study.* Neurology, 2014. **83**(5): p. 406-12.
21. Hughes, A.J., et al., *Accuracy of clinical diagnosis of idiopathic Parkinson's disease: a clinico-pathological study of 100 cases.* J Neurol Neurosurg Psychiatry, 1992. **55**(3): p. 181-4.
22. Booij, J. and R.J. Knol, *SPECT imaging of the dopaminergic system in (premotor) Parkinson's disease.* Parkinsonism Relat Disord, 2007. **13 Suppl 3**: p. S425-8.
23. Brooks, D.J., *Imaging approaches to Parkinson disease.* J Nucl Med, 2010. **51**(4): p. 596-609.
24. Eckert, T., et al., *FDG PET in the differential diagnosis of parkinsonian disorders.* Neuroimage, 2005. **26**(3): p. 912-21.
25. Eckert, T., et al., *Regional metabolic changes in parkinsonian patients with normal dopaminergic imaging.* Mov Disord, 2007. **22**(2): p. 167-73.
26. Eckert, T., C. Tang, and D. Eidelberg, *Assessment of the progression of Parkinson's disease: a metabolic network approach.* Lancet Neurol, 2007. **6**(10): p. 926-32.
27. Cummings, J.L., et al., *The role of dopaminergic imaging in patients with symptoms of dopaminergic system neurodegeneration.* Brain, 2011. **134**(Pt 11): p. 3146-66.

28. Farde, L., et al., *Substituted benzamides as ligands for visualization of dopamine receptor binding in the human brain by positron emission tomography.* Proc Natl Acad Sci U S A, 1985. **82**(11): p. 3863-7.
29. Pavese, N., et al., *In vivo assessment of brain monoamine systems in parkin gene carriers: a PET study.* Exp Neurol, 2010. **222**(1): p. 120-4.
30. Kazumata, K., et al., *Dopamine transporter imaging with fluorine-18-FPCIT and PET.* J Nucl Med, 1998. **39**(9): p. 1521-30.
31. Fazio, P., et al., *Quantitative Analysis of ^{18}F-(E)-N-(3-Iodoprop-2-Enyl)-2β-Carbofluoroethoxy-3β-(4'-Methyl-Phenyl) Nortropane Binding to the Dopamine Transporter in Parkinson Disease.* J Nucl Med, 2015. **56**(5): p. 714-20.
32. Darcourt, J., et al., *EANM procedure guidelines for brain neurotransmission SPECT using (123)I-labelled dopamine transporter ligands, version 2.* Eur J Nucl Med Mol Imaging, 2010. **37**(2): p. 443-50.
33. Prunier, C., et al., *Quantification of dopamine transporter by 123I-PE2I SPECT and the noninvasive Logan graphical method in Parkinson's disease.* J Nucl Med, 2003. **44**(5): p. 663-70.
34. Antonini, A., et al., *The status of dopamine nerve terminals in Parkinson's disease and essential tremor: a PET study with the tracer [11-C]FE-CIT.* Neurol Sci, 2001. **22**(1): p. 47-8.
35. Ribeiro, M.J., et al., *Dopaminergic function and dopamine transporter binding assessed with positron emission tomography in Parkinson disease.* Arch Neurol, 2002. **59**(4): p. 580-6.
36. Hall, H., et al., *Visualization of the dopamine transporter in the human brain postmortem with the new selective ligand [125I]PE2I.* Neuroimage, 1999. **9**(1): p. 108-16.
37. DeLorenzo, C., et al., *Modeling considerations for in vivo quantification of the dopamine transporter using [(11)C]PE2I and positron emission tomography.* J Cereb Blood Flow Metab, 2009. **29**(7): p. 1332-45.
38. Hirvonen, J., et al., *Measurement of striatal and extrastriatal dopamine transporter binding with high-resolution PET and [11C]PE2I: quantitative modeling and test-retest reproducibility.* J Cereb Blood Flow Metab, 2008. **28**(5): p. 1059-69.
39. Jucaite, A., et al., *Quantitative analyses of regional [11C]PE2I binding to the dopamine transporter in the human brain: a PET study.* Eur J Nucl Med Mol Imaging, 2006. **33**(6): p. 657-68.
40. Emond, P., D. Guilloteau, and S. Chalon, *PE2I: a radiopharmaceutical for in vivo exploration of the dopamine transporter.* CNS Neurosci Ther, 2008. **14**(1): p. 47-64.

41. Jucaite, A., et al., *Reduced midbrain dopamine transporter binding in male adolescents with attention-deficit/hyperactivity disorder: association between striatal dopamine markers and motor hyperactivity.* Biol Psychiatry, 2005. **57**(3): p. 229-38.
42. Ciumas, C., et al., *Reduced dopamine transporter binding in patients with juvenile myoclonic epilepsy.* Neurology, 2008. **71**(11): p. 788-94.
43. Zheng, M., et al., *Safety, pharmacokinetic, and positron emission tomography evaluation of serotonin and dopamine transporter occupancy following multiple-dose administration of the triple monoamine reuptake inhibitor BMS-820836.* Psychopharmacology (Berl), 2015. **232**(3): p. 529-40.
44. DeLorenzo, C., et al., *SEP-225289 serotonin and dopamine transporter occupancy: a PET study.* J Nucl Med, 2011. **52**(7): p. 1150-5.
45. Seki, C., et al., *Quantitative analysis of dopamine transporters in human brain using [11C]PE2I and positron emission tomography: evaluation of reference tissue models.* Ann Nucl Med, 2010. **24**(4): p. 249-60.
46. Leroy, C., et al., *Striatal and extrastriatal dopamine transporter in cannabis and tobacco addiction: a high-resolution PET study.* Addict Biol, 2011.
47. Odano, I., et al., *Quantitative PET analyses of regional [(11)C]PE2I binding to the dopamine transporter - Application to juvenile myoclonic epilepsy.* Neuroimage, 2012. **59**(4): p. 3582-93.
48. Ribeiro, M.J., et al., *A multitracer dopaminergic PET study of young-onset parkinsonian patients with and without parkin gene mutations.* J Nucl Med, 2009. **50**(8): p. 1244-50.
49. McKhann, G.M., et al., *The diagnosis of dementia due to Alzheimer's disease: recommendations from the National Institute on Aging-Alzheimer's Association workgroups on diagnostic guidelines for Alzheimer's disease.* Alzheimers Dement, 2011. **7**(3): p. 263-9.
50. Dubois, B., et al., *Advancing research diagnostic criteria for Alzheimer's disease: the IWG-2 criteria.* Lancet Neurol, 2014. **13**(6): p. 614-29.
51. Klunk, W.E., et al., *Imaging brain amyloid in Alzheimer's disease with Pittsburgh Compound-B.* Ann Neurol, 2004. **55**(3): p. 306-19.
52. Jack, C.R., et al., *Brain β-amyloid load approaches a plateau.* Neurology, 2013. **80**(10): p. 890-6.
53. Arriagada, P.V., et al., *Neurofibrillary tangles but not senile plaques parallel duration and severity of Alzheimer's disease.* Neurology, 1992. **42**(3 Pt 1): p. 631-9.
54. Okamura, N., et al., *Tau PET imaging in Alzheimer's disease.* Curr Neurol Neurosci Rep, 2014. **14**(11): p. 500.

55. Villemagne, V.L., et al., *Tau imaging: early progress and future directions.* Lancet Neurol, 2015. **14**(1): p. 114-24.
56. Saint-Aubert, L., et al., *Tau PET imaging: present and future directions.* Mol Neurodegener, 2017. **12**(1): p. 19.
57. Lockhart, S.N., et al., *Dynamic PET Measures of Tau Accumulation in Cognitively Normal Older Adults and Alzheimer's Disease Patients Measured Using [18F] THK-5351.* PLoS One, 2016. **11**(6): p. e0158460.
58. Kimura, Y., et al., *PET Quantification of Tau Pathology in Human Brain with 11C-PBB3.* J Nucl Med, 2015. **56**(9): p. 1359-65.
59. Hahn, A., et al., *Modeling Strategies for Quantification of In Vivo 18F-AV-1451 Binding in Patients with Tau Pathology.* J Nucl Med, 2017. **58**(4): p. 623-631.
60. Okamura, N., et al., *Novel 18F-labeled arylquinoline derivatives for noninvasive imaging of tau pathology in Alzheimer disease.* J Nucl Med, 2013. **54**(8): p. 1420-7.
61. Halldin, C., et al., *[(11)C]PE2I: a highly selective radioligand for PET examination of the dopamine transporter in monkey and human brain.* Eur J Nucl Med Mol Imaging, 2003. **30**(9): p. 1220-30.
62. Svarer, C., et al., *MR-based automatic delineation of volumes of interest in human brain PET images using probability maps.* Neuroimage, 2005. **24**(4): p. 969-79.
63. Koch, W., et al., *Clinical Testing of an Optimized Software Solution for an Automated, Observer-Independent Evaluation of Dopamine Transporter SPECT Studies.* Journal of Nuclear Medicine, 2005. **46**(7): p. 1109-1118.
64. Teune, L.K., et al., *Typical cerebral metabolic patterns in neurodegenerative brain diseases.* Mov Disord, 2010. **25**(14): p. 2395-404.
65. Akaike, H., *A New Look at the Statistical Model Identification.* IEEE Transactions on Automatic Control, 1974. **19**(6): p. 716-723.
66. Schwarz, G., *Estimating the dimension of a model.* Annals of Statistics, 1978. **6**(2): p. 461-464.
67. Yaqub, M., et al., *Evaluation of tracer kinetic models for analysis of [18F]FDDNP studies.* Mol Imaging Biol, 2009. **11**(5): p. 322-33.
68. Catafau, A.M. and E. Tolosa, *Impact of dopamine transporter SPECT using 123I-Ioflupane on diagnosis and management of patients with clinically uncertain Parkinsonian syndromes.* Mov Disord, 2004. **19**(10): p. 1175-82.
69. Volkow, N.D., et al., *Dopamine transporters decrease with age.* J Nucl Med, 1996. **37**(4): p. 554-9.
70. Shingai, Y., et al., *Age-related decline in dopamine transporter in human brain using PET with a new radioligand [^{18}F]FE-PE2I.* Ann Nucl Med, 2014. **28**(3): p. 220-6.

71. Emond, P., et al., *Synthesis and ligand binding of nortropane derivatives: N-substituted 2beta-carbomethoxy-3beta-(4'-iodophenyl)nortropane and N-(3-iodoprop-(2E)-enyl)-2beta-carbomethoxy-3beta-(3',4'-disubstituted phenyl)nortropane. New high-affinity and selective compounds for the dopamine transporter.* J Med Chem, 1997. **40**(9): p. 1366-72.
72. Rodriguez-Vieitez, E., et al., *Comparability of [18F]THK5317 and [11C]PIB blood flow proxy images with [18F]FDG positron emission tomography in Alzheimer's disease.* J Cereb Blood Flow Metab, 2017. **37**(2): p. 740-749.
73. Ng, K.P., et al., *Monoamine oxidase B inhibitor, selegiline, reduces (18)F-THK5351 uptake in the human brain.* Alzheimers Res Ther, 2017. **9**(1): p. 25.
74. Lemoine, L., et al., *Cortical laminar tau deposits and activated astrocytes in Alzheimer's disease visualised by (3)H-THK5117 and (3)H-deprenyl autoradiography.* Sci Rep, 2017. **7**: p. 45496.
75. Lemoine, L., et al., *Comparative binding properties of the tau PET tracers THK5117, THK5351, PBB3, and T807 in postmortem Alzheimer brains.* Alzheimers Res Ther, 2017. **9**(1): p. 96.
76. Chiotis, K., et al., *Imaging in-vivo tau pathology in Alzheimer's disease with THK5317 PET in a multimodal paradigm.* Eur J Nucl Med Mol Imaging, 2016. **43**(9): p. 1686-99.
77. Hostetler, E.D., et al., *Preclinical Characterization of 18F-MK-6240, a Promising PET Tracer for In Vivo Quantification of Human Neurofibrillary Tangles.* J Nucl Med, 2016. **57**(10): p. 1599-1606.
78. Villemagne, V.L., et al., *Imaging tau and amyloid-beta proteinopathies in Alzheimer disease and other conditions.* Nat Rev Neurol, 2018.

Appendix A

Age-related dopamine transporter availability measured using [^{11}C]PE2I PET

Introduction

[^{11}C]PE2I is a positron emission tomography (PET) ligand with high affinity and selectivity for the dopamine transporter (DAT). Decreased DAT availability is associated with various neurological disorders such as Parkinson's disease. We have recently shown that an 80 min dynamic [^{11}C]PE2I PET scan can be used for differential diagnosis of patients with parkinsonian disorder, (Paper II). For routine clinical application, we have validated the use of shorter acquisition times, with DAT availability estimated using standard uptake value ratio (SUVR)-1 at 30-40 min p.i. (Paper III). Age-related decline of DAT availability has previously been investigated with PET using [^{18}F]FE-PE2I, showing a reduction of striatal DAT of about 7% per decade as measured with BP_{ND}. The purpose of this study was to investigate the age-related changes of DAT availability measured with [^{11}C]PE2I PET using both BP_{ND} and SUVR-1 estimates.

Materials and Methods

Thirty healthy controls (HC) were included, age 20-67 years, as given in Supplemental Table 1. Each subject underwent an 80 min dynamic PET scan after injection of 350-400 MBq [^{11}C]PE2I. Each subject also received a T1-weighted MRI scan, for structural information, to be co-registered to the PET scan. Volumes of interest (VOIs) were defined on the MRI image applying an automated probabilistic VOI template (PVElab).

Supplemental Table 1. Mean age ± standard deviation (SD) and numbers of males and females included in each age-group.

Age-group	Number of HC (males / females)	Mean age ± SD
20-30	6 (3 / 3)	24 ± 2
30-40	6 (3 / 3)	33 ± 2
40-50	7 (3 / 4)	44 ± 3
50-60	5 (4 / 1)	54 ± 3
60-70	6 (3 / 3)	65 ± 2

Parametric BP_{ND} images were calculated using receptor parametric mapping (RPM) for the full 80 min data set and SUVR-1 images were calculated for a 30-40 min time window. Cerebellar grey matter was used as reference region. BP_{ND} and SUVR-1 values in caudate and putamen were retrieved from the parametric images by projecting the MRI-based VOIs, mean of left and right side. Relation between the BP_{ND} and SUVR-1 values and age was assessed using linear regression and mean changes per decade were calculated.

Results

The relationships between age and DAT availability measured with BP_{ND} and SUVR-1 are given in Supplemental Figure 1. A decrease of BP_{ND} was found in both caudate and putamen with 7.6 and 2.5 % mean decrease per decade respectively, although the decrease was only significant in caudate ($p<0.05$). A significant decrease was also found for SUVR-1 values in caudate, 6.2 % per decade, while no age-related effect on SUVR-1 values was observed in putamen.

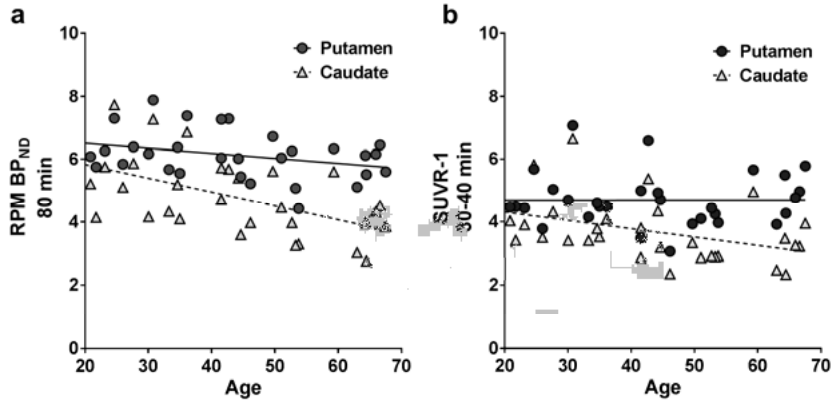

Supplemental Figure 1. Relationship between age and a) 80 min BP_{ND} and b) 30-40 min SUVR-1, in putamen and caudate.

Discussion

The decline of 7.6 % of DAT availability per decade in caudate, measured with BP_{ND}, is in line with previous studies. When estimating DAT availability with SUVR-1 on a 30-40 min interval the age-related decrease is lower, which may be explained by the previously demonstrated underestimation of SUVR-1 compared to BP_{ND} which decreases with decreasing BP_{ND} values (Paper III). Our result regarding the non-significant decline of DAT in putamen deviates from previous studies and needs further investigation. While using these methods for clinical assessment of DAT availability, age effects need to be considered for both BP_{ND} and SUVR-1 values in caudate.

Acta Universitatis Upsaliensis

Digital Comprehensive Summaries of Uppsala Dissertations from the Faculty of Medicine 1429

Editor: The Dean of the Faculty of Medicine

A doctoral dissertation from the Faculty of Medicine, Uppsala University, is usually a summary of a number of papers. A few copies of the complete dissertation are kept at major Swedish research libraries, while the summary alone is distributed internationally through the series Digital Comprehensive Summaries of Uppsala Dissertations from the Faculty of Medicine. (Prior to January, 2005, the series was published under the title "Comprehensive Summaries of Uppsala Dissertations from the Faculty of Medicine".)

Distribution: publications.uu.se
urn:nbn:se:uu:diva-341786

ACTA
UNIVERSITATIS
UPSALIENSIS
UPPSALA
2018